



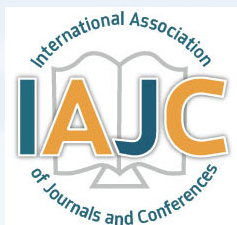
FALL / WINTER 2023  
VOLUME 15, NUMBER 2

Print ISSN: 2152-4157  
Online ISSN: 2152-4165

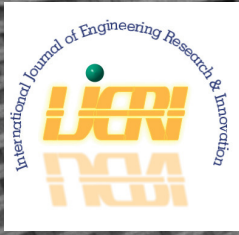
WWW.IJERI.ORG

# International Journal of Engineering Research & Innovation

**Editor-in-Chief: Mark Rajai, Ph.D.**  
**California State University Northridge**



Published by the  
**International Association of Journals & Conferences**



[www.ijeri.org](http://www.ijeri.org)

Print ISSN: 2152-4157  
Online ISSN: 2152-4165



[www.iajc.org](http://www.iajc.org)

# INTERNATIONAL JOURNAL OF ENGINEERING RESEARCH AND INNOVATION

## **ABOUT IJERI:**

- IJERI is the second official journal of the International Association of Journals and Conferences (IAJC).
- IJERI is a high-quality, independent journal steered by a distinguished board of directors and supported by an international review board representing many well-known universities, colleges, and corporations in the U.S. and abroad.
- IJERI has an impact factor of **1.58**, placing it among an elite group of most-cited engineering journals worldwide.

## **OTHER IAJC JOURNALS:**

- The International Journal of Modern Engineering (IJME)  
For more information visit [www.ijme.us](http://www.ijme.us)
- The Technology Interface International Journal (TIIJ)  
For more information visit [www.tiij.org](http://www.tiij.org)

## **IJERI SUBMISSIONS:**

- Manuscripts should be sent electronically to the manuscript editor, Dr. Philip Weinsier, at [philipw@bgsu.edu](mailto:philipw@bgsu.edu).

For submission guidelines visit  
[www.ijeri.org/submissions](http://www.ijeri.org/submissions)

## **TO JOIN THE REVIEW BOARD:**

- Contact the chair of the International Review Board, Dr. Philip Weinsier, at [philipw@bgsu.edu](mailto:philipw@bgsu.edu).

For more information visit  
[www.ijeri.org/editorial](http://www.ijeri.org/editorial)

## **INDEXING ORGANIZATIONS:**

- IJERI is indexed by numerous agencies. For a complete listing, please visit us at [www.ijeri.org](http://www.ijeri.org).

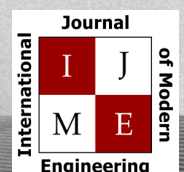
## **Contact us:**

**Mark Rajai, Ph.D.**

Editor-in-Chief  
California State University-Northridge  
College of Engineering and Computer Science  
Room: JD 4510  
Northridge, CA 91330  
Office: (818) 677-5003  
Email: [mrajai@csun.edu](mailto:mrajai@csun.edu)



[www.tiij.org](http://www.tiij.org)



[www.ijme.us](http://www.ijme.us)

---

# INTERNATIONAL JOURNAL OF ENGINEERING RESEARCH AND INNOVATION

The INTERNATIONAL JOURNAL OF ENGINEERING RESEARCH AND INNOVATION (IJERI) is an independent and not-for-profit publication, which aims to provide the engineering community with a resource and forum for scholarly expression and reflection.

IJERI is published twice annually (fall and spring issues) and includes peer-reviewed research articles, editorials, and commentary that contribute to our understanding of the issues, problems, and research associated with engineering and related fields. The journal encourages the submission of manuscripts from private, public, and academic sectors. The views expressed are those of the authors and do not necessarily reflect the opinions of the IJERI editors.

## EDITORIAL OFFICE:

Mark Rajai, Ph.D.  
Editor-in-Chief  
Office: (818) 677-2167  
Email: [ijmeeditor@iajc.org](mailto:ijmeeditor@iajc.org)  
Dept. of Manufacturing Systems  
Engineering & Management  
California State University-  
Northridge  
18111 Nordhoff Street  
Northridge, CA 91330-8332

## THE INTERNATIONAL JOURNAL OF ENGINEERING RESEARCH AND INNOVATION EDITORS

### *Editor-in-Chief:*

**Mark Rajai**

California State University-Northridge

### *Production Editor:*

**Philip Weinsier**

Bowling Green State University-Firelands

### *Manuscript Editor:*

**Philip Weinsier**

Bowling Green State University-Firelands

### *Publisher:*

**Bowling Green State University Firelands**

### *Web Administrator:*

**Saeed Namyar**

Advanced Information Systems

### *Technical Editors:*

**Andrea Ofori-Boadu**

North Carolina A&T State University

**Michelle Brodke**

Bowling Green State University-Firelands

**Marilyn Dyrud**

Oregon Institute of Technology

**Mandar Khanal**

Boise State University

**Chris Kluse**

Bowling Green State University

**Zhaochao Li**

Morehead State University

---

# TABLE OF CONTENTS

<i>Editor's Note: Registration is now open for the 9<sup>th</sup> IAJC international conference in Orlando, Florida</i> .....	3
Philip Weinsier, IJERI Manuscript Editor	
<i>Comparison of 3D Scanning Techniques and Photogrammetry Tools</i> .....	5
Noah Burchett, Western Kentucky University	
<i>Simulation of Robotic Gaits Using a Single Degree of Freedom Leg</i> .....	15
Andrew J. Wasson, Kettering University; Diane L. Peters, Kettering University; Yaomin Dong, Kettering University	
<i>Automated Water Bottle Packaging System</i> .....	28
Maged Mikhail, Mateusz Plachta, and Adalberto Acosta, Purdue University Northwest	
<i>Autonomous Aquaculture Water Quality Monitoring System</i> .....	35
Jade Chapman, Texas A&M University; Kevin Zhang, Texas A&M University; Gage Arter, Texas A&M University; Truc Le, Texas A&M University; Dr. Rainer Fink, Texas A&M University; Dr. Ben Zoghi, Texas A&M University	
<i>Instructions for Authors: Manuscript Submission Guidelines and Requirements</i> .....	43



# 9<sup>TH</sup> IAJC INTERNATIONAL CONFERENCE

[www.2024.iajc.org](http://www.2024.iajc.org)

OCTOBER 10-13, 2024 – ORLANDO, FLORIDA

The leading indexed high-impact-factor conference on engineering and related technologies.



## CALL FOR CONFERENCE PROPOSALS

Conference Submission Deadlines:

- Abstract and Poster Submissions                      March 22, 2024
- Full-Paper Submissions (optional)                      April 26, 2024

Full papers may be submitted after a related abstract has been accepted for presentation. All full papers will automatically be reviewed for publication in the conference proceedings and the high-impact-factor IAJC journals after the conference. All submissions must be made using our [online system](https://2024.iajc.org/registration) (<https://2024.iajc.org/registration>).

Have questions or need help? Contact Philip Weinsier (Conference General Chair) at [philipw@bgsu.edu](mailto:philipw@bgsu.edu)



---

## Editorial Review Board Members

Mohammed Abdallah	State University of New York (NY)	Basile Panoutsopoulos	Community College of Rhode Island (RI)
Paul Akangah	North Carolina A&T State University (NC)	Shahera Patel	Sardar Patel University (INDIA)
Nasser Alaraje	Michigan Tech (MI)	Thongchai Phairoh	Virginia State University (VA)
Ali Alavizadeh	Purdue University Northwest (IN)	Huyu Qu	Broadcom Corporation
Lawal Anka	Zamfara AC Development (NIGERIA)	Desire Rasolomampionona	Warsaw University of Tech (POLAND)
Jahangir Ansari	Virginia State University (VA)	Michael Reynolds	University of West Florida (FL)
Sanjay Bagali	Acharya Institute of Technology (INDIA)	Nina Robson	California State University-Fullerton (CA)
Kevin Berisso	Ohio University (OH)	Marla Rogers	C Spire
Sylvia Bhattacharya	Kennesaw State University (GA)	Dale Rowe	Brigham Young University (UT)
Monique Bracken	University of Arkansas Fort Smith (AR)	Anca Sala	Baker College (MI)
Tamer Breakah	Ball State University (IN)	Alex Sergejev	Michigan Technological University (MI)
Michelle Brodke	Bowling Green State University (OH)	Mehdi Shabaninejad	Zagros Oil and Gas Company (IRAN)
Shaobiao Cai	Penn State University (PA)	Hiral Shah	St. Cloud State University (MN)
Rajab Challoo	Texas A&M University Kingsville (TX)	Natalie Shah	Florida Institute of Technology (FL)
Isaac Chang	Illinois State University (IL)	Deepa Sharma	
Shu-Hui (Susan) Chang	Iowa State University (IA)	Mojtaba Shivaie	Shahrood University of Technology (IRAN)
Rigoberto Chinchilla	Eastern Illinois University (IL)	Musibau Shofoluwe	North Carolina A&T State University (NC)
Phil Cochrane	Indiana State University (IN)	Jiahui Song	Wentworth Institute of Technology (MA)
Curtis Cohenour	Ohio University (OH)	Carl Spezia	Southern Illinois University (IL)
Emily Crawford	Claflin University (SC)	Michelle Surerus	Ohio University (OH)
Z.T. Deng	Alabama A&M University (AL)	Harold Terano	Camarines Sur Polytechnic (PHILIPPINES)
Marilyn Dyrud	Oregon Institute of Technology (OR)	Sanjay Tewari	Missouri University of Science & Techn (MO)
Mehran Elahi	Elizabeth City State University (NC)	Vassilios Tzouanas	University of Houston Downtown (TX)
Ahmed Elsayy	Tennessee Technological University (TN)	Jeff Ulmer	University of Central Missouri (MO)
Cindy English	Millersville University (PA)	Abraham Walton	University of South Florida Polytechnic (FL)
Ignatius Fomunung	University of Tennessee Chattanooga (TN)	Haoyu Wang	Central Connecticut State University (CT)
Ahmed Gawad	Zagazig University (EGYPT)	Jyhwen Wang	Texas A&M University (TX)
Hamed Guendouz	Yahia Fares University (ALGERIA)	Boonsap Witchayangkoon	Thammasat University (THAILAND)
Kevin Hall	Western Illinois University (IL)	Shuju Wu	Central Connecticut State University (CT)
Mamoon Hammad	Abu Dhabi University (UAE)	Baijian "Justin" Yang	Purdue University (IN)
Bernd Haupt	Penn State University (PA)	Eunice Yang	University of Pittsburgh Johnstown (PA)
Rodward Hewlin	University of North Carolina Charlotte (NC)	Xiaoli (Lucy) Yang	Purdue University Northwest (IN)
Youcef Himri	Safety Engineer in Sonelgaz (ALGERIA)	Hao Yi	Chongqing University (CHINA)
Delowar Hossain	City University of New York (NY)	Faruk Yildiz	Sam Houston State University (TX)
Xiaobing Hou	Central Connecticut State University (CT)	Yuqiu You	Ohio University (OH)
Shelton Houston	University of Louisiana Lafayette (LA)	Hong Yu	Fitchburg State University (MA)
Ying Huang	North Dakota State University (ND)	Pao-Chiang Yuan	Jackson State University (MS)
Christian Bock-Hyeng	North Carolina A&T University (NC)	Afshin Zahraee	Purdue University Northwest (IN)
Pete Hylton	Indiana University Purdue (IN)	Jinwen Zhu	Missouri Western State University (MO)
John Irwin	Michigan Tech (MI)		
Toqeer Israr	Eastern Illinois University (IL)		
Alex Johnson	Millersville University (PA)		
Rex Kanu	Purdue Polytechnic (IN)		
Reza Karim	North Dakota State University (ND)		
Manish Kewalramani	Abu Dhabi University (UAE)		
Tae-Hoon Kim	Purdue University Northwest (IN)		
Chris Kluse	Bowling Green State University (OH)		
Doug Koch	Southeast Missouri State University (MO)		
Mohan Krishna	Vidyavardhaka College of Eng. (INDIA)		
Resmi Krishnankuttyrema	Bowling Green State University (OH)		
Zaki Kuruppallil	Ohio University (OH)		
Shiyong Lee	Penn State University Berks (PA)		
Soo-Yen (Samson) Lee	Central Michigan University (MI)		
Chao Li	Florida A&M University (FL)		
Jiliang Li	Purdue University Northwest (IN)		
Zhaochao Li	Morehead State University (KY)		
Neil Littell	Ohio University (OH)		
Dale Litwhiler	Penn State University (PA)		
Albert Lozano-Nieto	Penn State University (PA)		
Mani Manivannan	ARUP Corporation		
G.H. Massiha	University of Louisiana (LA)		
Thomas McDonald	University of Southern Indiana (IN)		
David Melton	Eastern Illinois University (IL)		
Kay Rand Morgan	Mississippi State University (MS)		
Sam Mryyan	Excelsior College (NY)		
Jessica Murphy	Jackson State University (MS)		
Arun Nambiar	California State University Fresno (CA)		
Rungun Nathan	Penn State Berks (PA)		
Aurenice Oliveira	Michigan Tech (MI)		
Troy Ollison	University of Central Missouri (MO)		
Reynaldo Pablo	Purdue Fort Wayne (IN)		

# COMPARISON OF 3D SCANNING TECHNIQUES AND PHOTOGRAMMETRY TOOLS

Noah Burchett, Western Kentucky University

## Abstract

Digital reproduction of complex shapes, such as fossils, skulls, sculptures, and other flowing geometries, is difficult. Optical methods such as 3D scanning and photogrammetry allow for capturing such complex geometry that is nearly impossible to reproduce otherwise. Once 3D models are available, rapid prototyping (3D printing) allows for scalable and reproducible models quite easily. Three methods of capturing these geometries were evaluated in this study: two scanning systems and one photogrammetric camera software. The Revopoint 3D POP is a structured light scanner used in conjunction with a PC or mobile device, utilizing feature detection as the scanner is moved around the object, capturing a reasonable level of detail at the cost of an unrefined mesh. The Matter and Form V2 3D Scanner uses a built-in turntable to scan subjects with a laser line as they rotate. The multiple scans captured were merged to form a single digital model. 3DF Zephyr is a photogrammetry software used to build a digital model from a series of photographs taken of the sample in question. Digital photos were taken using an Olympus OM-D E-M5II in a rising spiral fashion and then combined to create a 3D digital model. Human faces, statues, and concrete fragments were used to evaluate these techniques. The final results were 3D printed on the Ender 3 V2 for visual comparison. The goal was to increase the use of 3D scanning technology available to the university community.

## Introduction

As engineers, the environment one operates in is important in most, if not all, applications. One way to visualize this working environment is to model it, most commonly using computer aided drafting (CAD) programs, such as Solidworks or Autodesk products. However, complex geometries can arise that prolong this modeling process and produce errors in these models that can complicate the design process down the road. To mitigate this problem, accurate models can be created using alternate means, such as scanning and photogrammetry. Fields ranging from biology and medicine to criminology and real estate all utilize this skill to recreate entities for research, law enforcement, business, and more. These methods are also used in aerospace, automotive, video game, and other industries to produce fast and accurate three-dimensional models. One outlet for these models is 3D printing, whether it be a resin or fused deposition modeling (FDM) printer to reproduce these items in miniature to larger sizes.

In the early stages of this study, a literature review was conducted to find papers discussing the scanners and methods used, but most papers only considered one system to objects but not each other. In this current study, the author hoped to broaden interest in advanced 3D modeling tools, find a relatively cheap solution for universities to invest in, and show multiple objects being scanned by the three products and how they compared. The goal of this study was not to test the manufacturer's claims on the precision of the digitized model produced but rather to report the possibilities and limitations of each system.

## Criteria

In this paper, the author covers a series of scanners that were procured at different price points. The Revopoint POP 3D (Revopoint, 2021) is at the lower end of the price range observed, at approximately \$550, with the Matter and Form V2 scanner (Matter and Form, 2018) bringing the middle up to a price of \$750. Finally, photogrammetry is rather fluid in terms of hardware and software costs. The free version of the 3DF Zephyr software (3DF Zephyr, 2022) was used for photogrammetry in conjunction with an Olympus OM-D E-M5II camera with a Panasonic Lumix G Vario 1: 3.5-5.6 / 14-42mm lens. The total cost was estimated to be approximately \$1000. This range was chosen as it was decided to be a small investment for labs or student prototyping centers to spend for future endeavors in 3D modeling and printing.

After acquiring a point cloud of the subject, it would then be exported out to a Standard Tessellation Language format (also known as a .stl file) where it would be processed by Ultimaker Cura (Braam, 2022) with presets of a 0.16mm-layer height and a set infill of 30% Gyroid. All the models produced were compared after being printed on an Ender-3 V2 with the same modifications used on all prints, including an upgraded bed, leveled printing surface, and upgraded aluminum extruder. Supports generated by Cura were removed and any residual markings from the removal tools or process were then blended with the rest of the model via light exposure to heat introduced by a blowtorch. Filament and hue were kept constant using MatterHackers red polylactic acid (PLA) for most models, but variants in color appeared in some cases and were concluded to not impact the comparison of the models. Additionally, differences in the coloration of 3D models were present but impacted results superficially.

---

## Background

3D scanners work using the principle of emitting a light that can reflect off the subject after which the displacement or voids of light are then transformed into varying depths. The scanner then reconstructs the object digitally, recreating 3-dimensional objects in a 2-dimensional plane by accounting for the reliefs of the subject and analyzing the deformation. The Revopoint POP 3D Scanner and Matter and Form V2 3D Scanner are both structured-light scanners that use a small webcam in tandem with projectors to observe the distortion of horizontal and vertical bands of emitted rays. The collected individual scans are then merged; the Revopoint does so automatically (Revopoint, 2021), whereas the Matter and Form V2 3D Scanner must be operated manually using a base scan (Matter and Form, 2018). This process arguably gives more user input, but can also lead to shrunken or misaligned models. Photogrammetry operates on a similar principle by taking overlapping photos and stitching them together, based on camera location, distance, discernable features, and triangulation. All of these methods work on the same principle, gathering key points between observations or pictures and storing them in a dense point cloud. Once the capture of data is complete, the area in between the points is meshed with straight areas and a solid is formed. With more points, features like curves and complex geometries can be meshed with ease, whereas lesser points in the cloud lead to blocky or choppier features. This mesh can then be saved to other programs to be 3D printed.

## Revopoint POP 3D

The Revopoint POP 3D scanner is a lightweight structured light scanner that detects features by introducing infrared light that safely bounces off the subject. The device is constructed of two IR sensors on each side of the camera with an RGB sensor for texture information (Revopoint, 2021). The device can be connected via USB A or USB C to a personal computer or mobile smartphone to power the device and transmit captured data. To use the Revopoint POP, two pieces of software were used: Handy Scan and Handy Studio (during the writing of this paper, Revopoint released a new suite of tools, including Revo Scan, Studio, and Calibrate, that were not available during the conceptual or data-collection phases of this report) (Revopoint, 2021). Handy Scan allows for communication between the scanner and the PC to collect data from the scanner, save the generated point cloud, or export a mesh to a Wavefront OBJ File or a Stanford Triangle Format (.obj or .ply, respectfully) format. Handy Studio is used to edit the saved .obj or .ply file, as it can mesh, clip, fill, smooth, mirror, and export the subject to a .stl format (Revopoint, 2021). The exported .stl file is then processed by Cura to print on the Ender 3. The Revopoint POP 3D scanner offers five distinct modes of scanning: Features, Marker, Face, Body, and Dark/Hair. The Features mode scans objects with distinct shape features, such as sculptures or figures.

Marker mode scans objects with fewer distinct features, such as flat boards, balls, or bowls. Markers must be distributed evenly on the subject as the scanner generates point cloud data from the pattern of adjacent markers. Face mode is used to scan human faces, where exposure and gain are set according to face skin reflectivity. Body mode is best at scanning human bodies with gain and exposure being set automatically for the subject. Dark mode, which has the added title of Hair, can scan some dark objects such as boxes and clothes but not objects such as black leather shoes that absorb most light. All of these are available for the corresponding mobile phone version of Handy Scan, which connects over a local mobile phone's hotspot, except for the Marker mode. The scanner captures eight frames per second while operating and automatically merges the frames of data as it goes. The subject being scanned can be stationary or placed on the included turntable with fiducial targets that allow the subject to turn. In terms of editing, Handy Scan allows users to completely erase the entire scan or the latest grouping of frames. Handy Studio allows users to clip the model via a drawn plane, fill any voids either by a curved or planar surface, smooth a mesh, or mirror the mesh. The editing abilities of the software are limited in that it cannot select individual points. This tool would be useful for erasing one protruding error, as a small noise can break models rather than having to restart the scan from scratch if saved incorrectly.

## The Matter and Form V2

The Matter and Form V2 scanner is a structured light scanner, akin to the Revopoint POP 3D, but implements the use of two Class 1 Lasers (as defined by IEC60825-1:2007) (Matter and Form, 2018). The device is a foldable system with one portion folding out to reveal the built-in 7" (approximately 18 cm) turntable on one side and the laser/webcam assembly on the other. The scanning assembly is located on a threaded shaft that turns to raise to 9.8" (approximately 25 cm) and lower the scanner, as the subject turns incrementally to scan all sides. An additional stipulation, the object cannot weigh more than 6.6 lbs. (3.0 kg). The software MF Studio has settings to scan at five fixed height intervals and control the rotation of the table. Multiple scans are taken, cleaned, and merged. The resulting mesh can then be exported to .ply, .obj, or .stl formats locally.

To merge, the user manually overlays a secondary scan over a base scan and aligns it to the best of his or her ability. Selecting a different base scan can result in different alignments. MF Studio can be upgraded using the software +Quickscan, an add-on that can limit scanning to one laser and rotate the turntable constantly during a scan. It can reduce a usual hour-long scan down to five minutes. This decreases the overall operating time, but leaves more noise to filter through after scanning. The editing tools available are plentiful and helpful, as they offer a plentiful variety to control and reconfigure scans.



---

The brush tool selects and deselects points that can be deleted (referred to as “cleaning”). The brush tool works akin to a laser or drill: it has a set radius and will bore through everything in its path. This can be resolved by turning the scan and deselecting points that are to be kept. The program also features an adjustable noise filter that can select points within a certain noise radius. Lastly, MF Studio contains three different cropping tools: a radial tool and two plane erasure tools. The radial tool narrows the selection radius of points the higher it is turned. The plane tools erase data from the lowest point up (upward plane) or erase data from the tallest point down (downward plane). Whereas the Revopoint POP 3D has five different modes for scanning a multitude of surfaces, the Matter and Form V2 scanner has just one regular scan mode. Additionally, the instruction manual suggests avoiding metallic, reflective, clear, or dark surfaces, as they might not be captured.

## Photogrammetry (3DF Zephyr Software)

Photogrammetry consists of three key components: photo, -gram, -metry. Photo relates to how the subject is recorded (via a photographic picture), the ending -gram refers to something being written or drawn, and the suffix -metry means to measure. In essence, photogrammetry means to measure the subject by connecting or drawing a series of images together. Any device capable of capturing and storing pictures can be used; in this current study, an Olympus OM-D E-M5II was used, due to its high resolution of 16 or 40 MP. While other methods have a stationary sensor or camera to observe a rotating object, photogrammetry involves rotating the camera while the subject remains stationary. The photos of a given subject are taken in an upwards spiral fashion, as it is optimal for capturing details in complex and obtuse geometries. With the ever-increasing resolution of cameras installed in smartphones, this method can be easily introduced to all who can upload photos to the program.

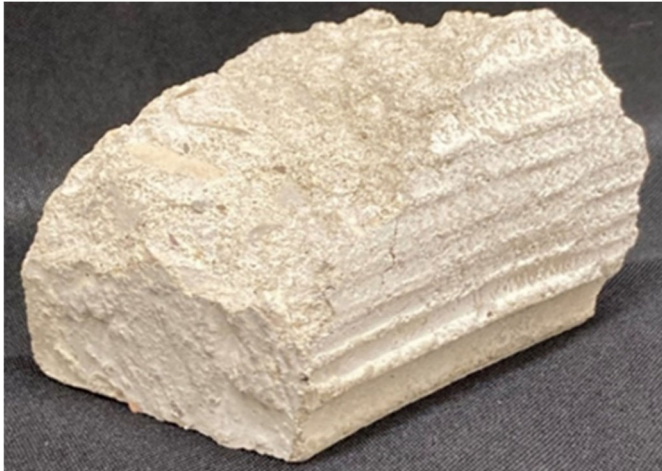
3DF Zephyr is a software package that takes the sequence of photos taken of a subject and searches for matches between each picture to build a 3D mesh (3DF Zephyr, 2022). The free version was used in this study, in spite of its limited editing and exporting tools, when compared to paid versions, and can only handle up to 50 pictures at a time for reconstruction. In constructing and meshing the point cloud data, any unpictured or sparsely photographed features will be tessellated, thus exaggerating the missing space, or making it appear jagged or abstract. To edit the generated model, 3DF Zephyr offers multiple smoothing options, filling holes selectively or being watertight, and a plethora of clipping tools. These clipping tools use a plane, a box, a polygonal boundary, points from the cloud, camera viewpoints, triangles, or colors to edit the subject. The program can quickly measure and display characteristics like distance, elevation change, and inclination. Measurements can be used to determine the scaling factor between the sample and the model and can help edit a mesh closer to real propor-

tions. This method may potentially produce models with altered dimensions, due to its imprecision, but results can be improved by calibrating the camera used with a measuring rod.

## Examples

The format of the following images will first show the subject before showing the digitized model from each method, with additional notes in the sequence: Revopoint POP 3D, Matter and Form V2, and finally photogrammetry. The first sample examined was a concrete cornice trim fragment chosen due to its low reflectivity, textured top and sides, and flat bottom that could rest on a turntable or observation platform. Figure 1 shows the subject. The two structured light scanners, the Revopoint POP 3D and the Matter and Form V2, were used in conjunction with a box composed of a cardboard shell lined with black foam to perform scans. The black foam absorbed any light and limited outside interruptions. The box was light-sealed so that the uncovered sections of the cardboard box would not be detected by the scanners. The Revopoint POP 3D had no issues arise during the scanning process for this sample. The adjustable tripod holding the scanner made obtaining various views simple, as it was a matter of simply adjusting the level while the sample turned on the table. While the texture mapping made it harder to see the level of detail, the roughness of the rising middle section (denoted by the red solid circle in Figure 2) was more rounded than the real subject. In addition, the bottom-most groove (denoted by the blue dashed circle in Figure 2) was completely missing, making the model shorter than the sample by two millimeters. Figure 2 shows the model with highlights.

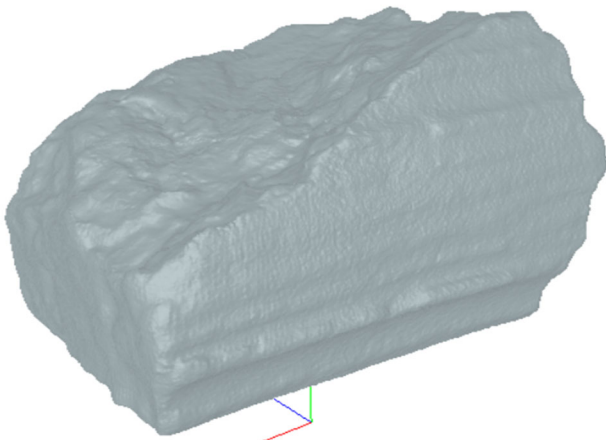
The Matter and Form V2 scanner had no issues arise in the scanning of this piece. The sample was set on a wooden block during the scanning process and then edited out afterward; this was done in order to allow for better capture of the subject’s underside. The side grooves were softer than the previous sample, but show more detail in the middle rock section (once again denoted by a red solid circle in Figure 3), whereas the Revopoint POP 3D’s model was overall rounder. Additionally, it had a more accurate height, but reduced width of approximately one to two millimeters along the profile. Figure 3 shows the digitized model from this scanner. For photogrammetry, the sample was placed on a wooden observation platform with the photos taken in a circular and then rising pattern. The observation platform (a wooden stool) was used because it allowed the photographer to have easy rotation around the subject and allowed for the camera to have a constant radius away from the subject in the case of the circular pictures. The pattern allowed for the most capture of detail in the fewest number of pictures. 3DF Zephyr rejected no pictures and used all of the data in its reconstruction of this sample. In Figure 1(d), some amounts of the wooden platform can be seen underneath the model, as the software filled the holes by drawing on old textures.



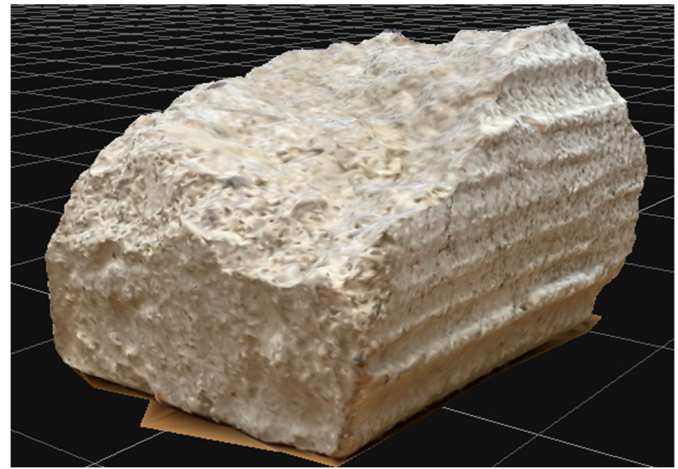
(a) The original concrete cornice trim fragment.



(b) The Revopoint POP 3D model.



(c) The Matter and From V2 model.



(d) The 3DF Zephyr model.

Figure 1. The first subject is a concrete cornice trim fragment, with digitized models.

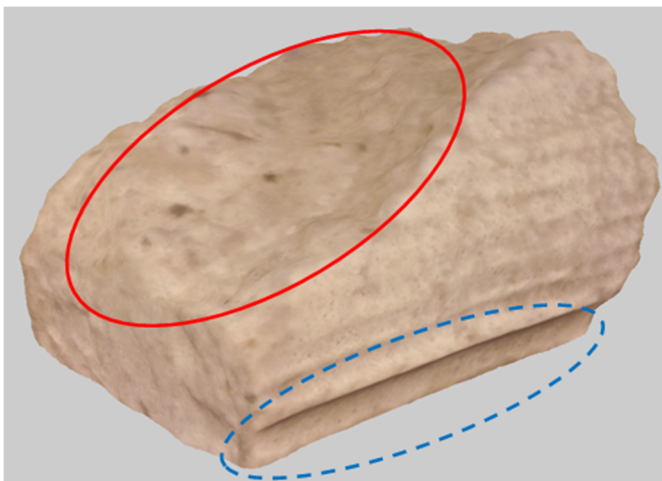


Figure 2. The Revopoint POP 3D model of the concrete cornice trim fragment with textures and highlighted sections.

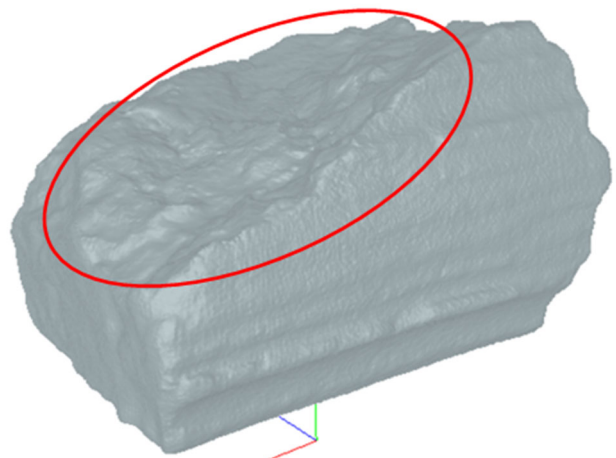


Figure 3. The Matter and Form V2 model of the concrete cornice trim fragment with highlights.

The 3D printed model was significantly smaller than the original, at an estimated 75% scale of the original sample. What it lacks in dimensions, the model makes up for in detail as it has a greater level of detail than the Matter and Form V2 scanner's mesh. It can be complimented for its textures as seen in the figure, as it looks much closer to the original sample than the other models. The next sample was a fragment of a tombstone statue that had a child holding onto an angel's hand. This sample was chosen due to its low reflectivity and more complex geometries and pits (in comparison to the concrete cornice trim). Figure 4 shows that the hand has a natural curved palm that leads to the clutched thumb: this is a natural location to check for tessellations in the scanners. While not easily seen, the fingers and curved surfaces have pits and chips that provide another spot to check for accuracy among the models. The Revopoint POP 3D had minimal issues arise during the process of scanning the fragment. The only inconvenience was that the tripod could not be placed so it could have an overhead view to

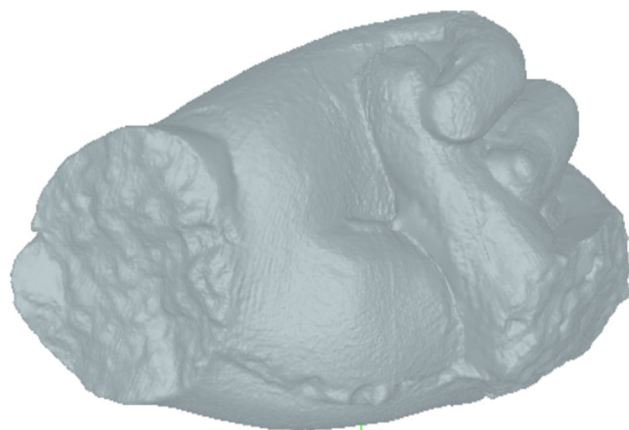
catch the beneficial details of the model. To achieve this viewing angle, the operator picked up the tripod assembly and maneuvered it to the angles and recesses of the hand while the scanner was running. The final 3D print shows that minimal detail was lost and eradicated the texture coloring issue seen. Some noteworthy spots include exposed rocks and broken smoothed sections. Figure 4(b) shows the finished model with its off-color texturing. The Matter and Form V2 scanner had minimal issues in the scanning process as well. The limited motion of the table helped in some regards and hurt in others, as shorter scans allowed for faster data capturing. However, the mounted, nonadjustable camera led to issues orienting the sample to obtain more data in smaller parts; Figure 5 shows this in that the crease where the thumb and the palm meet has significant tessellation, and which can also be seen in the area encompassed by the red circle. Additionally, the fingers had tessellations along their digits and several of the pits and recesses were partially to mostly filled in the final print.



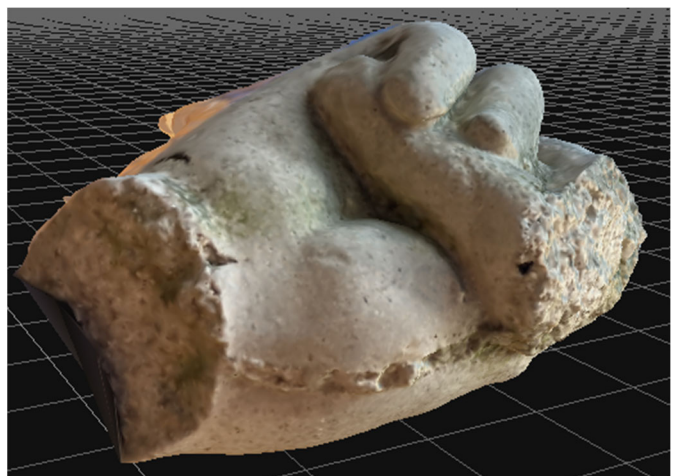
(a) The sample concrete statue fragment.



(b) The Revopoint POP 3D model.



(c) The Matter and From V2 model.



(d) The 3DF Zephyr model.

Figure 4. The second subject is a concrete statue fragment with digitized models.

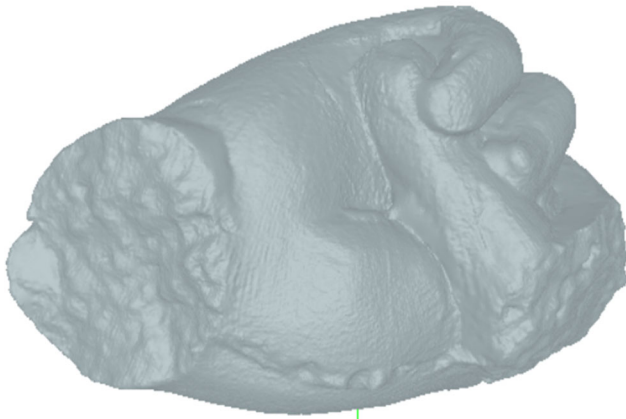


Figure 5. The Matter and Form V2 model with highlights around the tessellation between the thumb and the palm.

It was difficult to acquire photos of the hand statue fragment for photogrammetry. This was mostly due to the wooden stool having a recessed seat on which the fragment sat, allowing the sample to rock and become reoriented while taking pictures. To combat this problem, clay was introduced to the base of the hand to hold it upright, at the cost of detail at the base; Figure 6 shows this using the clay-filled hole that resulted in a crescent shape (shown with the yellow dashed circle) of data missing in the final model. Additionally, some major tessellations can be seen as fins sprouting on the backside of the model for no discernable reason. The final print also shows that the size was much closer to the original than the cornice trim. Additionally, there was significant tessellation due to 3DF Zephyr rejecting some data and the fact that black clay was used to hold the hand in an upright position. Some of the tessellations can be seen on the left side of Figure 6, where the black clay was removed along with the portion of the hand that contained rejected data.

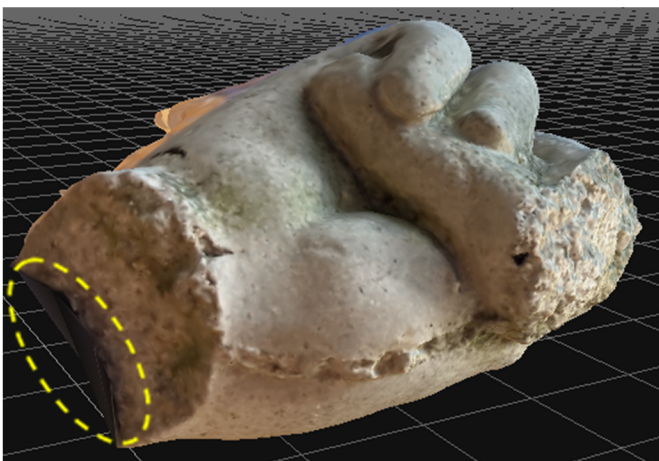


Figure 6. Photogrammetry model of the concrete statue fragment with General/Deep Presets with highlighted lack of concise data due to clay.

The last set of samples analyzed for this study was a series of statues located around Western Kentucky University's campus: a rabbit statue, a book statue, a running fountain, and the school's mascot, Big Red. Figure 7 shows these along with some notes indicating that the inscription on the fountain is only in appearance and is not physically engraved. Due to its design, Matter and Form V2 could not scan these samples. While the Revopoint POP 3D scanner was marketed as useable indoors and out, in reality outdoor lighting conditions severely interfered with the infrared sensor. Scanning of these statues was attempted in sunny, cloudy, shaded, rainy, and snowy conditions but no data could be collected with the mobile or desktop version of the software. Future attempts to test Revopoint's abilities outdoors could include scanning at night or creating a dark environment by enveloping the sample in a dark box created with a hunting blind and black tablecloth. Photogrammetry was able to handle all these statues with varying degrees of success. Figures 8-10 show the digitized rabbit statue, book statue, and fountain, while Figure 11 shows the effects of the different settings in 3DF Zephyr that facilitated differing Big Reds models. While the cornice trim and stone hand fragment were digitized using the "General" preset of settings, the outdoor setting and rejected photos from the data set led to the "Urban" preset. The first statue of rabbit statue Chauncey Too resulted in a satisfactory model, capturing details in the scenery, including the base with no distortion of the statue's original shape. Figure 8 shows the model trimmed of the surrounding environment.

The next statue, "Books For Father." was taken on the same day as the previous statue in similar weather conditions. However, their locations differed, as Chauncey Too was located in a dense section of trees that provided darker shading than the building shading "Books For Father." With these facts noted, the digitized model shows a significant level of detail with some minor discrepancies in the crevice where the two book "pages" meet and at the statue's base. Tessellation was present in the crevice of the pages resulting in a sphere, while the rest of the statue appeared as it otherwise did. Figure 9, at the bottom right corner, shows that the base has pits and jagged sections on all sides, likely due to the polished appearance of the base, which can be seen in Figure 7(b). Additionally, the "pages" were smooth on the sculpture whereas the final mesh was stippled and bumpy.

Figure 10 shows that the Guthrie Fountain, photographed later in the afternoon, had several points of interest in the final model. To begin, the top four smaller columns supporting the topmost water-collecting dish are separated by gaps whereas the model has tessellated that area closed. This was due to a lack of data around each of the individual columns, which could be remedied by increasing the picture limit, but then would run the risk of getting the equipment wet. The next point of interest was the water, one of the most difficult entities to digitize, which was running during the series of photographs. It is present in the model but comes at the cost of engulfing some pipes and structures underneath it.



(a) Chauncey Too by Jim Budish in 2007.



(b) "Books For Father" by Kevin Robb in 2008 outside of Gordon Wilson Hall.



(c) The Guthrie Fountain outside of Van Meter Hall.



(d) The Big Red statue sculpted by Russell Faxon in 1974.

*Figure 7.* Statues located around Western Kentucky University's campus.

The deep pit at the bottom right side of the fountain may be a product of the sun's glare, resulting in erroneous data at this area alone. Aside from these issues, the texturing looks superb. The final 3D print of the fountain shows intricate details of the bottom column, ridges, and swirls. One detail that could not be recreated with much success was the lettering "Western Kentucky University." As mentioned, the letters do not recess into the material and are thus harder to digitize, though it still makes a faint appearance in the final model.



Figure 8. Chauncey Too model in 3DF Zephyr with Urban/Deep Presets.

The next three models are used here in order to offer a brief explanation of 3DF Zephyr's settings. When creating a project, the settings are selected from a variety of options before any operations can commence. There are three kinds of settings categories for users: Presets, Advanced, and Custom (Custom settings were disregarded for this study for clarity). In Presets, a user can select a category and the level of detail for that operation. Users can choose between preset categories of General, Ariel, Urban, Human body, Surface scan, and Vertical structures, followed by the presets Fast, Default, and Deep in order to control speed. The user can choose these settings for camera orientation, dense point cloud collection, and surface reconstruction. Each category has certain advantages and disadvantages when compared, depending on the subject matter of the photogrammetry.

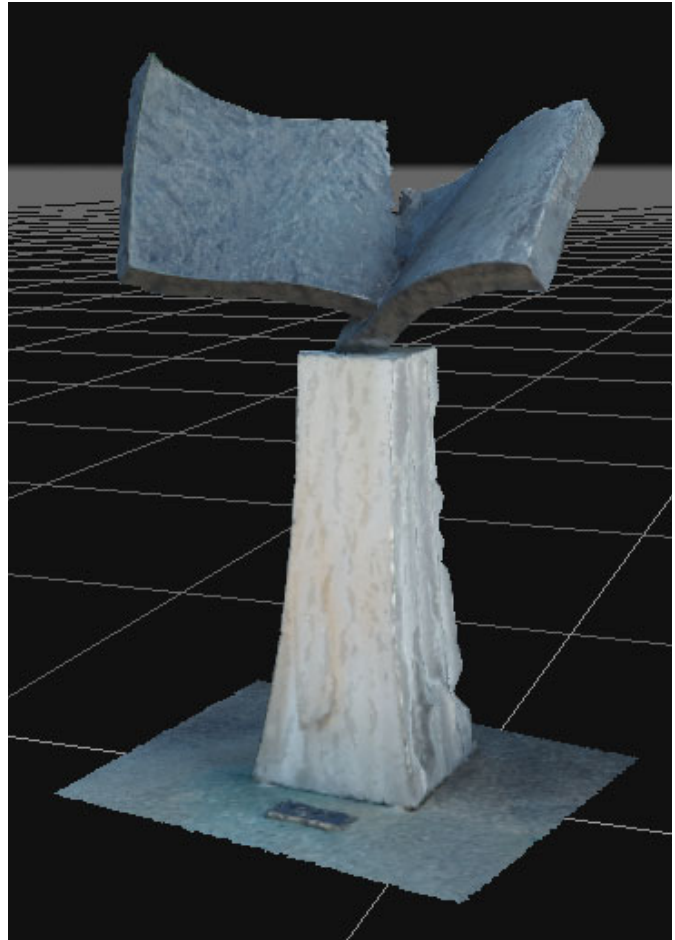


Figure 9. "Books For Father" model in 3DF Zephyr with Urban/Deep Presets.



Figure 10. Guthrie Fountain model in 3DF Zephyr with Urban/Deep Presets.

The Advanced options give a user more control of certain parameters in the digitizing process. As a trade, the more intense settings require more computing power and time. Figure 11 shows the models for the Big Red statue using photogrammetry. Several different settings were used, resulting in drastically different processing times, from five minutes to over an hour. The settings discussed here are those present in version 6.506 of 3DF Zephyr Free. The first model of Big Red was run using General presets with Deep detail levels to capture as much detail as possible in the fastest time. The operation for Figure 11(a) ran for a total of five minutes. Some tessellations and odd texturing can be seen in the right armpit, right hand, and mouth; otherwise, this model is excellent. The software did not accept the entirety of the data provided, which may be a case for the issues listed above. The next model of Big Red, Figure 11 (b), was run using Urban presets with Deep detail levels to capture as much detail as possible. The operation ran for a total of thirty minutes. This model fixed some of the issues of Figure 11(a), such as decreasing the tessellation of the right hand, right armpit, and mouth.

However, the model is significantly thinner than the original statue, when turned to the side. No discernable reason can be given, as the program accepted more of the photo set with the Urban preset than the General preset. Additionally, some tessellation can be seen on top of the head. The last model of Big Red, Figure 11(c), was created using the Advanced settings by maxing out possible features, such as key point sensitivity, matching type, and matching stage depth, while leaving all other parameters at their defaults. The resulting operation ran for a total of one hour and fifteen minutes. As can be seen, the program created a giant chest cavity, an array of ghost faces, and an elongated mouth wrapped around its head. The top of the head appears to have extreme tessellation whereas the hands and fingers

have been decreased to blobs. However, the backside of the Big Red model appears to be the best of the three. Additionally, the legs closely resemble the quality of the other two.

## Conclusions

All of these methods excel in different areas of 3D scanning and modeling: resolution, ease of scanning, model clean-up, processibility, and portability. For medium to larger sample scans taken indoors, the Revopoint POP 3D scanner excels, as its feature recognition alignment saves ample time taking multiple scans as well as offers different modes for scanning different sample types. Matter and Form V2 excels at scanning small objects. Its included software cleans the model faster than every other method. But, for most situations, indoors or out and small to large samples, photogrammetry is the most accessible method of modeling in comparison to the other tools mentioned in this paper. However, it relies heavily on focused, high-resolution pictures to create accurate models. With the issues arising in digitizing real objects, any of these systems are still advantageous to other labor-intensive methods with their low price point and barrier of entry. The downfalls of these methods are nothing more than the limited technology available to users. However, research should be conducted to find the optimal settings for each sample and how lighting conditions impact the final model. Lastly, expanding the reach of this research to include the Custom settings of 3DF Zephyr could provide additional insight as to how each mode compares. The addition of a new suite of tools from Revopoint holds promise as well as it may address the limitations of the editing tools discussed in this paper.

This technology advances with every passing quarter. For instance, Creality will soon release the CR-Lizard Scanner, which could offer better, more affordable scanning to the

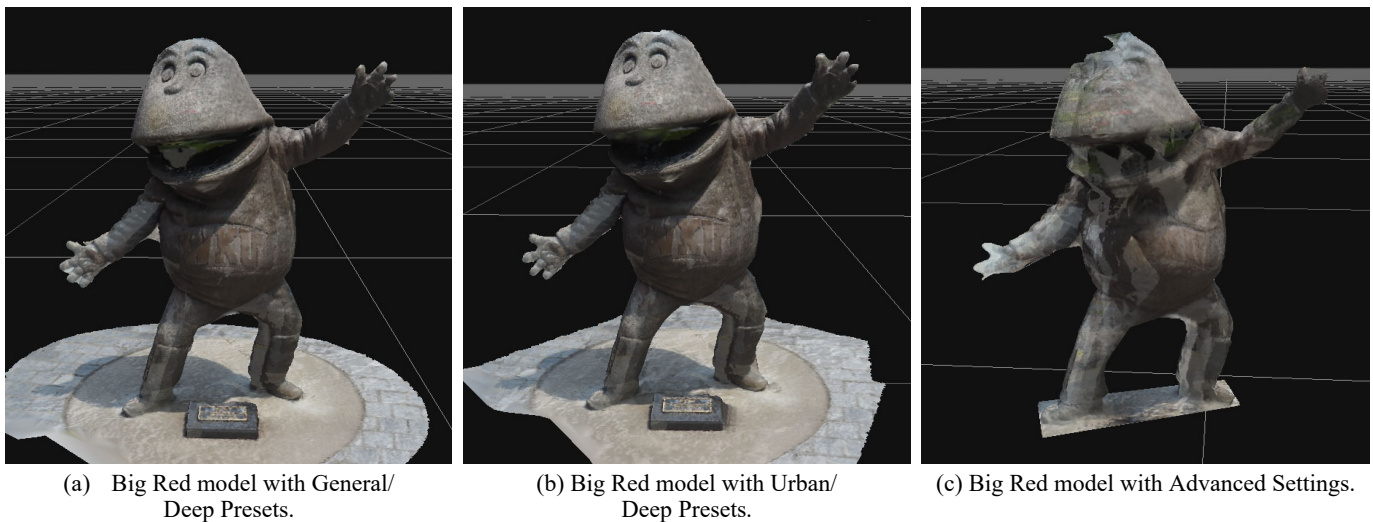


Figure 11. Big Red models made with different settings within 3DF Zephyr.

---

community at large. Additionally, Epic Games and their acquired company, Capturing Reality, have announced plans to release the app RealityScan to the public, which allows users to create high-fidelity 3D models that could be implemented with the Unreal Engine (Epic Games Introduces RealityScan App, Now in Limited Beta, 2022). The last major development during the writing of this paper was the newly announced Nvidia 3D MoMa, an AI approach with inverse rendering that will allow for smooth implementation of user-generated models into graphic engines to change parameters such as material, light sources, and added physics (Salian, 2022).

## Data Availability Statement

Data from this report, including photographs, digitized models, and Cura G-codes, will be made available upon request.

## Declaration of Competing Interests

The authors declare that they have no known competing financial interests or personal relationships that could have appeared to influence the work reported in this paper.

## Acknowledgments

This work was funded in part by James L. “Bud” Layne and his contributions to the Center for Project-based Learning at WKU. The author thanks many individuals who supported this study, including Wade Decker, Chloe Henson, and Darren Tinker. Additional thanks to Professor Joel Lenoir, who had the initial idea for this paper, encouraged me to pursue such a task, and allowed the digitization of multiple items found within his lab.

## References

- 3DF Zephyr (6.506). (2022). 3DFLOW. <https://www.3dflow.net/3df-zephyr-6-5-is-out-now/>
- Braam, D. (2022). Ultimaker Cura (4.13.1). Ultimaker. <https://ultimaker.com/learn/print-at-super-speed-with-ultimaker-cura-4-13/>
- Epic Games Introduces RealityScan App, Now in Limited Beta. (2022, April 4). Epic Games, Inc. <https://www.epicgames.com/site/en-US/news/epic-games-introduces-realityscan-app-now-in-limited-beta>
- Matter and Form. (2018). Matter and Form 3D Scanner V2 User Manual. [https://matterandform.net/downloads/MF\\_Studio\\_User-Manual\\_EN.pdf?2018-05-14](https://matterandform.net/downloads/MF_Studio_User-Manual_EN.pdf?2018-05-14)
- Revopoint. (2021). POP 3D SCANNER User Manual. [https://www.revopoint3d.com/wp-content/uploads/download/Revopoint%20POP%20User%20Manual\\_V2.2.0.pdf](https://www.revopoint3d.com/wp-content/uploads/download/Revopoint%20POP%20User%20Manual_V2.2.0.pdf)
- Salian, I. (2022, June 21). AI in the Big Easy: NVIDIA Research Lets Content Creators Improvise With 3D

Objects. NVIDIA. <https://blogs.nvidia.com/blog/2022/06/21/inverse-rendering-3d-research-cvpr/>

## Biographies

**NOAH PR BURCHETT** is a graduating senior in the Mechanical Engineering program at Western Kentucky University. Mr. Burchett will receive his BS in Mechanical Engineering from Ogden College in January of 2023 and plans to continue his education for a PhD. He has extensive experience in 3D modeling and interests in additive manufacturing, statistical analysis, and robotics. Mr. Burchett may be reached at [noah.burchett19@aol.com](mailto:noah.burchett19@aol.com)



# SIMULATION OF ROBOTIC GAITS USING A SINGLE DEGREE OF FREEDOM LEG

Andrew J. Wasson, Kettering University; Diane L. Peters, Kettering University; Yaomin Dong, Kettering University

## Abstract

In this paper, the authors present an analysis of three different gaits—diagonal gait, side gait, and front-back gait—for a quadrupedal robot. The specific robotic leg used in this work, first proposed by Peters and Chen (2014) and further developed by Jin (2015), was actuated with a double cam system. This work builds upon those studies by incorporating multiple legs of this type into a single robot before considering the overall system. The cams all turned at a constant speed throughout the duration of the simulation. This analysis was carried out using the dynamic simulation capabilities of the Dassault Systemès SolidWorks CAE software. Two of the three gaits were found to have issues balancing left to right, while the third had issues with balancing front to back. The first gait's balancing issues were judged to be issues that could be corrected, leading to the conclusion that it is a feasible gait for this robot. Those corrections will be explored in future work, as will the performance of a robot using this specific leg in a hexapod configuration.

## Introduction

Mobile robots can take many different forms and use different types of locomotion. In some cases, wheels or tracks are used. However, legs are also a possible method for robots to move themselves through the world. The advantage of using legged locomotion is that wheels require some sort of prepared surface to function best, and may not function at all in some types of terrain (Raibert, 1986). With the use of legs, a robot can step over some obstacles and traverse different types of terrain. Many robotic legs use multiple degrees of freedom and complicated control systems to move and interact with their surroundings, which has the advantage of giving them some degree of flexibility, beyond simply adjusting the timing between the legs (Joze, Habibi & Asadi, 2007; Herrero & Martinez, 2007).

However, there are legs that are far simpler in design and have correspondingly simpler control systems, such as hexapod locomotion systems (Buehler, Koditschek & Saranli, 2002; García-López, Gorrestieta-Hurtado, Vargas-Soto, Ramos-Arreguin, Sotomayor-Olmedo & Morales, 2012) or quadruped systems meant for running (Talebi, Poulakakis, Papadopoulos & Buehler, 2001). Other designs reported in the literature examined the impact of leg design on energy efficiency (Koutsoukis & Papadopoulos, 2021) or examined specifically the foot trajectory of a single leg (Koushik, Krishna, Rahul & Sreedharan, 2021).

Just as there are many different types of robotic legs, there are a variety of different gaits, or ways in which the different legs can move with respect to one another. Some of these gaits focus specifically on the motion of bipedal robots (Kurz, Judkins, Arellano & Scott-Pandorf, 2008; Collins & Ruina, 2005; Ha, Han & Hahn, 2007). These robots pose special challenges, as a bipedal robot is not stable in the absence of some form of control (Song & Waldron, 1989). As humans are bipedal creatures, much of the work in this current study was based on a study of human gait patterns, with the goal of implementing aspects of human walking in a robot. Running gaits or rapid locomotion gaits have also been considered (Cho & Kong, 2020; Liu & Ben-Tzvi, 2020).

There is also a significant body of work dealing with gaits that can be used with quadruped robots (Tsujita, Tsuchiya & Onat, 2001; Lewis & Bekey, 2002; Inagaki, Yuasa, Suzuki & Arai, 2006; Asci & Zhang, 2021), with the work by Inagaki et al. (2006) also applicable to robots with a greater number of legs. In many of these cases, a trotting gait was used (Spröwitz, Tuleu, Vespignani, Ajallooeian, Badri & Ijspeert, 2013; Zhang, Gao, Han, Chen & Han, 2014; Zhang, Rong, Hui, Li & Li, 2016; Fukuoka & Kimura, 2009). Such a gait is relatively fast, compared to walking, but can be more challenging to maintain stability. Other gaits considered were walking (Fukuoka & Kimura, 2009; Nagakubo & Hirose, 1994) and running (Nagakubo & Hirose, 1994; Poulakakis, Smith & Buehler, 2005). In addition, some studies focused specifically on the terrain that a quadruped robot can traverse (Raibert, Blankespoor, Nelson & Pflayter, 2008). The focus of this current study was on the performance of a specific robot with three different walking gaits: a diagonal gait, a side gait, and a front-back gait.

## Robotic Gaits

In this current study, three walking gaits were used—diagonal, side, and front-back. Each is briefly described, and a diagram is given to illustrate which legs are being used simultaneously. As they are walking gaits, there is always at least one leg, and in this case two legs, in contact with the ground at all times. Figure 1(a) shows the diagonal gait configuration, where the legs diagonally across from each other move at the same time. Legs in contact with the ground are represented by a black box, while a leg not contacting the ground is represented by white. The right front leg, therefore, is contacting the ground at the same time as the left back leg; when these legs are lifted, the left front leg and right back leg contact the ground. Figure 1(b) shows the side gait configuration, where the front and back legs on one

side of the robot move at the same time. The right front and back legs contact the ground at the same time, and the left front and back legs contact the ground, while the right legs are lifted. Figure 1(c) shows the front-back gait configuration, where the two front legs move together, and the two rear legs move together.

right front leg	■	□
left front leg	□	■
right back leg	□	■
left back leg	■	□

(a) Diagonal gait configuration.

right front leg	■	□
left front leg	□	■
right back leg	■	□
left back leg	□	■

(b) Side gait configuration.

right front leg	■	■
left front leg	■	■
right back leg	□	■
left back leg	□	■

(c) Front-back gait configuration.

Figure 1. Gait configurations.

## Description of System

Figure 2 shows the robot in a quadruped configuration with the cams mounted to the main body and one of the pieces of the leg attached to the main body to allow it to pivot. The main body of the robot is a hollow rectangular mass. The platform the robot walks on is a flat rectangular surface. The robot was modeled and simulated in Solidworks using the motion analysis tool. The legs were constrained to the cams, which were connected to the main body. Each gait was simulated for 50 seconds and at four different rotation rates for the cams. Five seconds after the start of the simulation, rotation was given to one set of legs, depending on the gait, followed five seconds later by a rotation provided to the other set of legs. The legs were controlled only in terms of how fast the cams were rotating and when they started rotating. After the initial start, rotation was never reduced or taken away from any pair of legs. The Cartesian coordinate system was set up so that the positive X direction would be to the right and the positive Y direction would be up. Figure 3 shows that the positive Z direction, considered forward, was perpendicular to the XY-plane pointing out of the page.

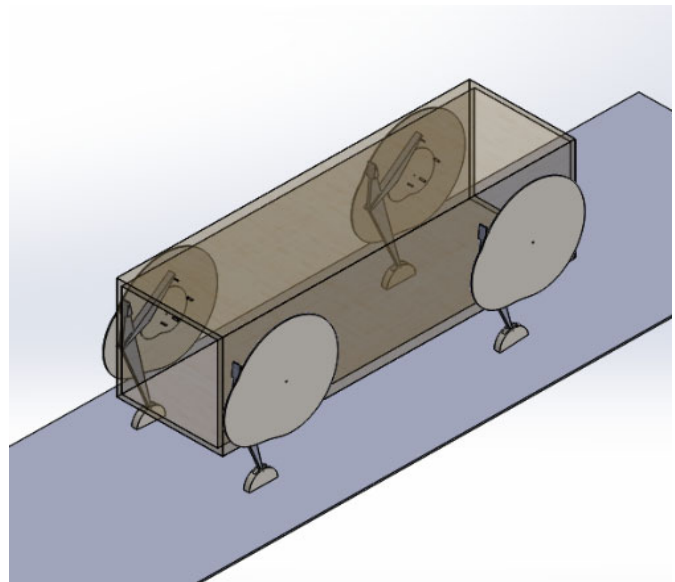


Figure 2. Robot configuration.

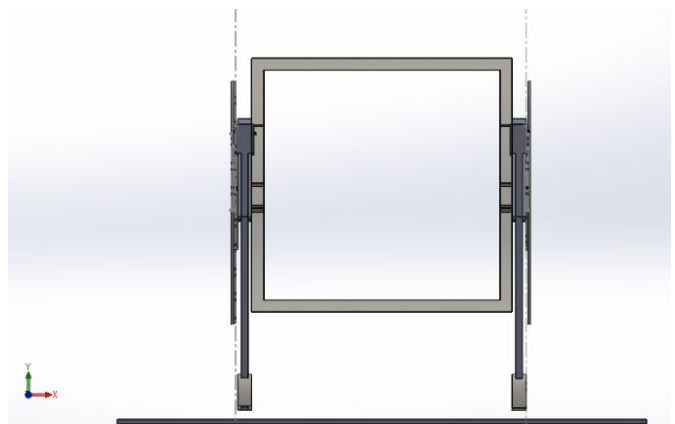


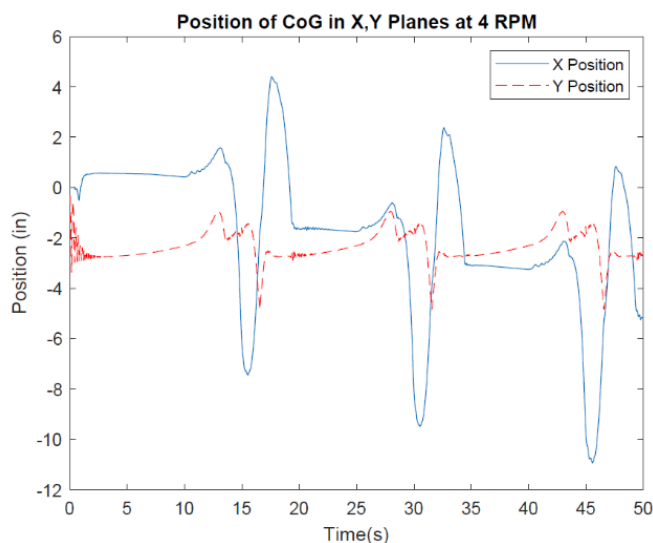
Figure 3. Coordinate system and front of robot.

The position, velocity, and acceleration of the center of gravity (CoG) of the main body were tracked and graphed in both the X and Y directions, with the CoG assumed to be in the exact center of the robot's body. The Z direction was tracked but was not graphed, as it only showed whether the robot moved forward or backwards, which was not relevant to how well the robot was able to support and balance itself. The robot sat about two inches above the platform. This was done to prevent clipping issues at the start of the simulation. During the first five seconds of the simulation, there were no control inputs in order to give the robot an opportunity to land on the platform, settle, and stop vibrating before locomotion began. Therefore, if any data points during the time period 0-5 seconds were abnormally large and reduced the readability of the graphs, those data points would be set to zero to increase the resolution of the actual data. This phenomenon was mainly seen in the velocity and acceleration graphs.

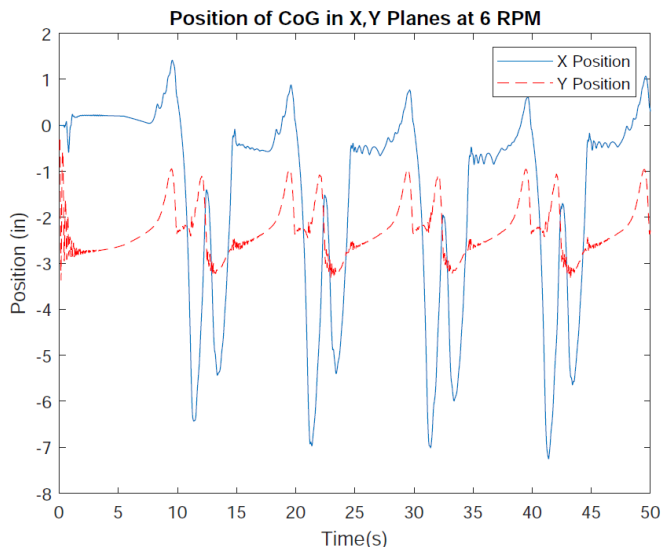
## Results

A variety of data were collected from the simulation, all specifically for the center of gravity (CoG) in order to evaluate the stability of the robot for each of the three gaits. Figure 4 shows the change in position of the center of gravity in the X direction over a cycle, in order, for the different speeds (in RPMs); these were 11.86", 7.85", 6.88", and 5.47". As RPM increased, there were diminishing returns on how much the change in position, or what could be considered the side-to-side sway of the robot, decreased. There also appeared to be a speed "breakpoint" between 8 RPM and

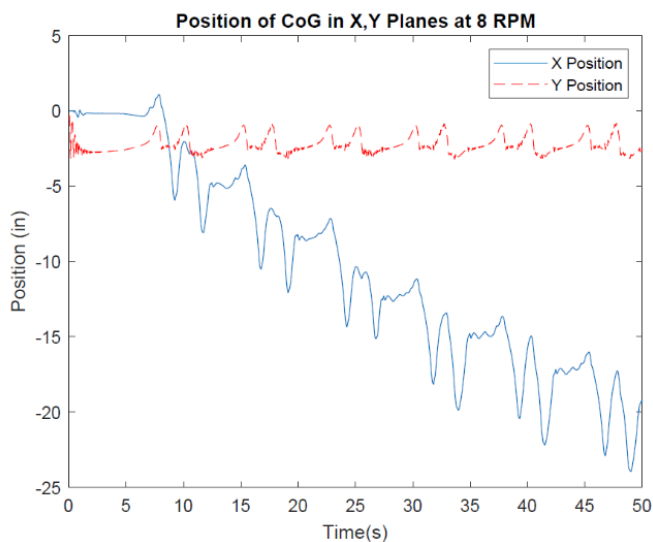
6 RPM, where the drift of the robot started earlier and was more pronounced. Figure 5 shows the velocity in both the X and Y directions for the position of the CoG at four different rotation rates for the diagonal gait. The velocity graphs have a pattern present in the 4 and 6 RPM graphs of there being a repeating cone shape for the Y direction where it may be vibrating when standing still and the velocity is dissipating. This pattern does not exist in the 10 and 8 RPM graphs. Another difference between the set of graphs is that the highest velocity in the 4 and 6 RPM graphs is recorded in the X direction, but the maximum velocities for 8 and 10 are in the Y direction.



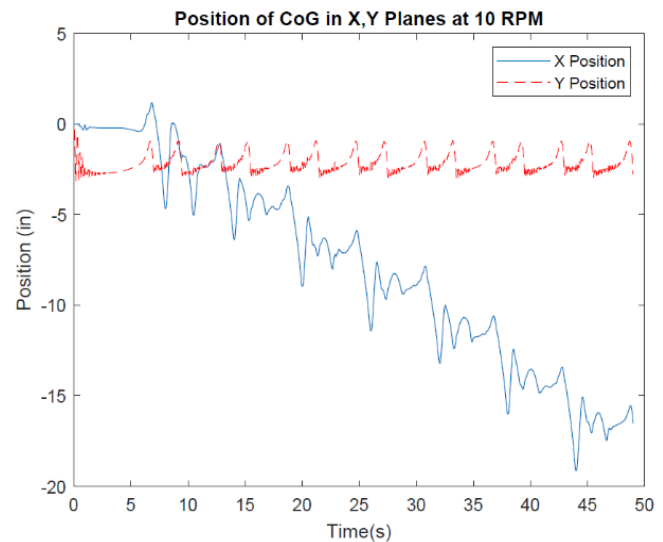
(a) X,Y planes at 4 RPM.



(b) X,Y planes at 6 RPM.

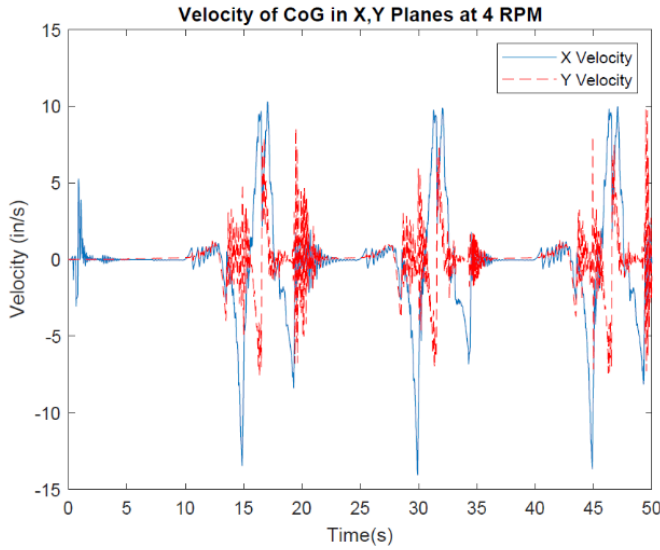


(c) X,Y planes at 8 RPM.

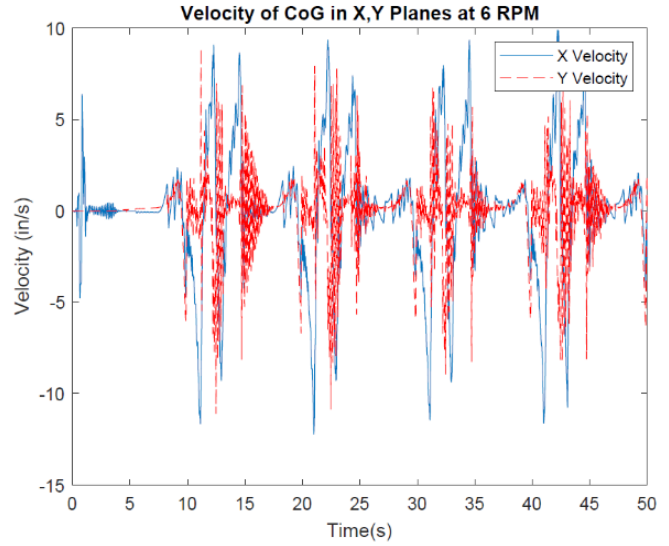


(d) X,Y planes at 10 RPM.

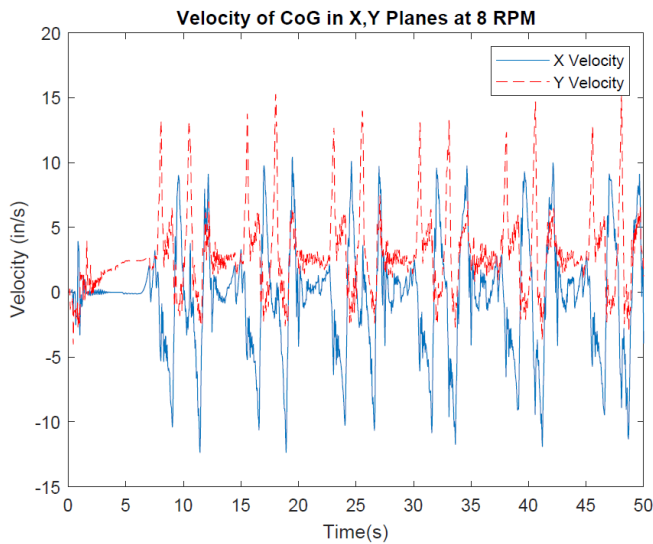
Figure 4. Position of CoG for the diagonal gait.



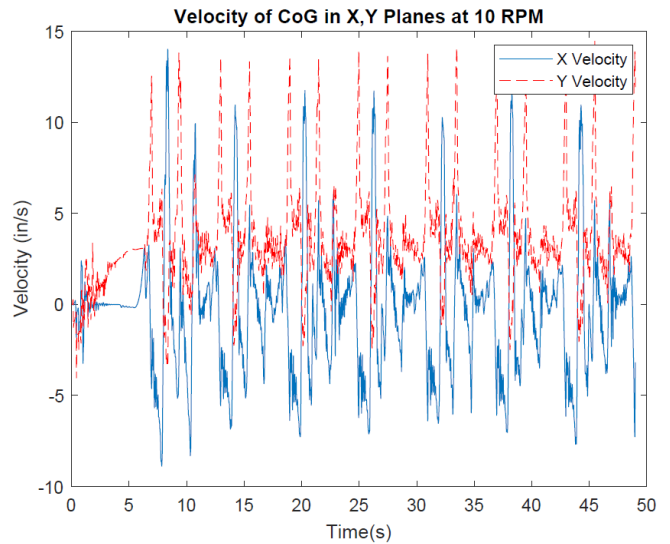
(a) X,Y planes at 4 RPM.



(b) X,Y planes at 6 RPM.



(c) X,Y planes at 8 RPM.

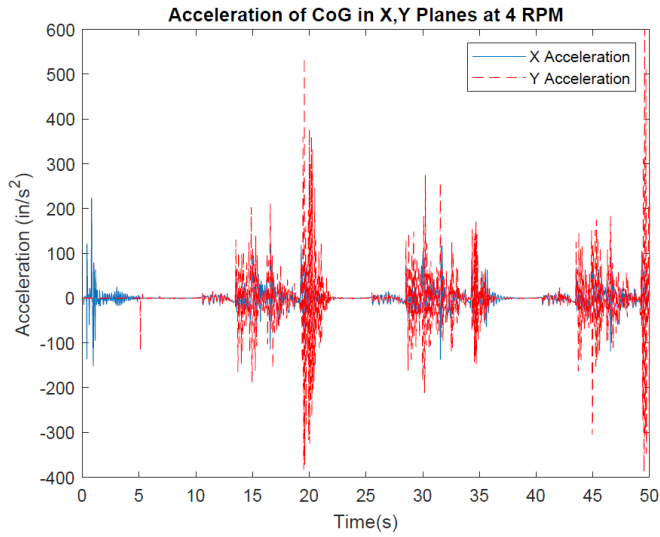


(d) X,Y planes at 10 RPM.

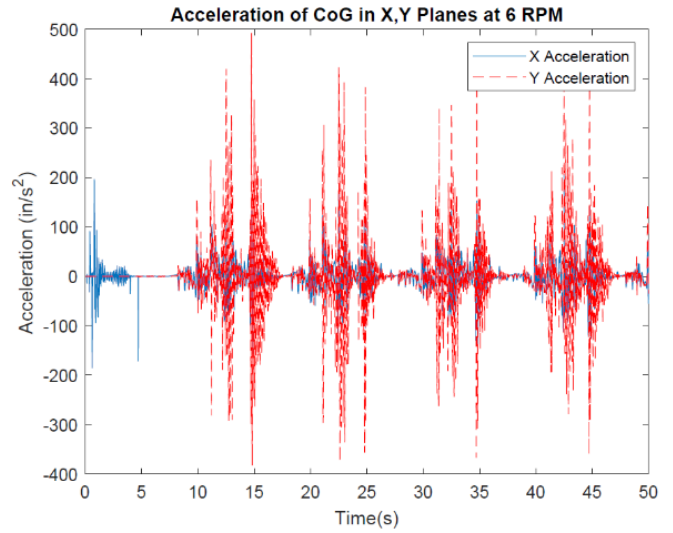
Figure 5. Velocity of CoG for the diagonal gait.

Figure 6 shows the acceleration in both the X and Y directions for the position of the CoG at four different rotation rates for the diagonal gait. The acceleration graphs all seem to have similar peak accelerations around  $500 \text{ in/s}^2$ , or 1.29Gs in the Y direction with the X direction having no relatively significant acceleration outside of the first five seconds. All four graphs also seem to only have this high rate of acceleration once during their motion. This may be due to Solidworks, or the simulation was not carried out long enough to see a pattern for these spikes. An attempt was made to run the simulation long enough to see a pattern; no such pattern appeared, and running for long

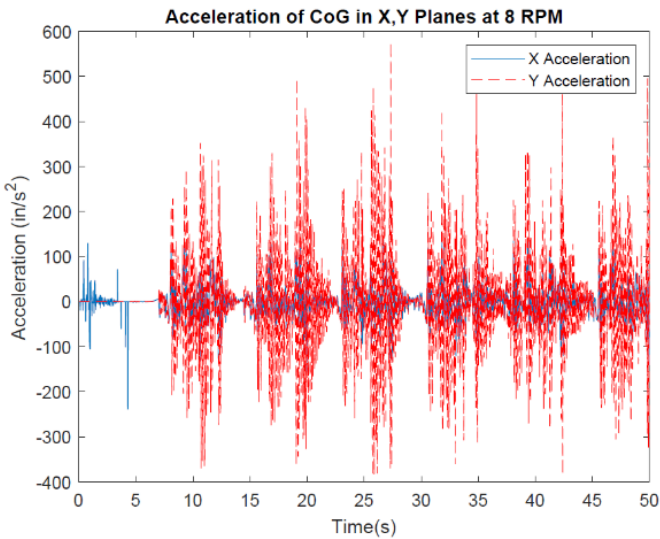
periods of time was computationally intensive. Figure 7 shows the position in both the X and Y directions for the position of the CoG at four different rotation rates for the side gait. Note that in the 8 and 10 RPM position graphs, there is a small spike inside of each valley. The significance of this spike was unclear; physical experimentation, with an actual model of the robot, could indicate whether it is a physical phenomenon or simply an artifact of simulation. The average motion in the X direction (sway) was around nine in all our graphs. This showed that for this gait, increasing the speed of the cams only increased the speed at which the robot walked forward.



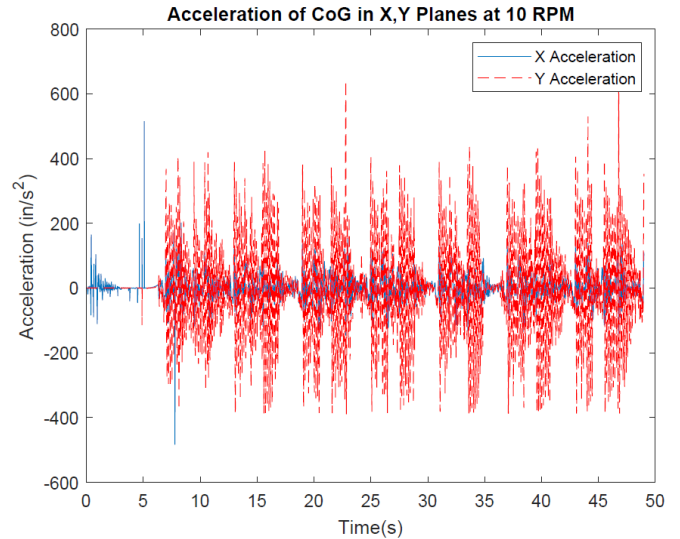
(a) X,Y planes at 4 RPM.



(b) X,Y planes at 6 RPM.

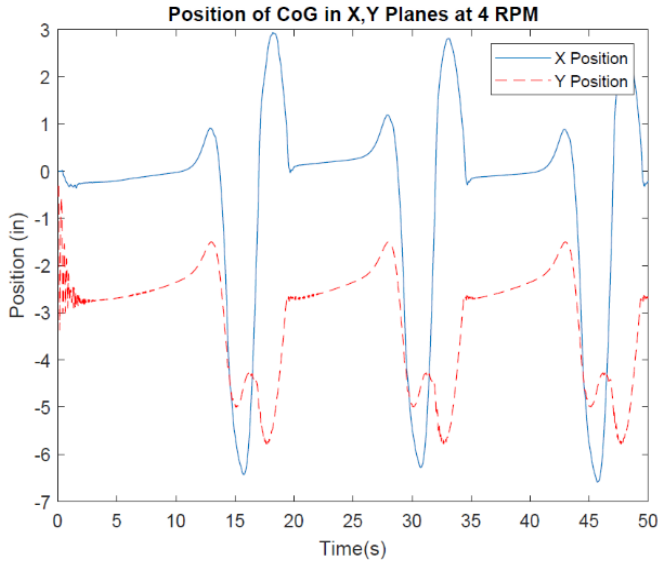


(c) X,Y planes at 8 RPM.

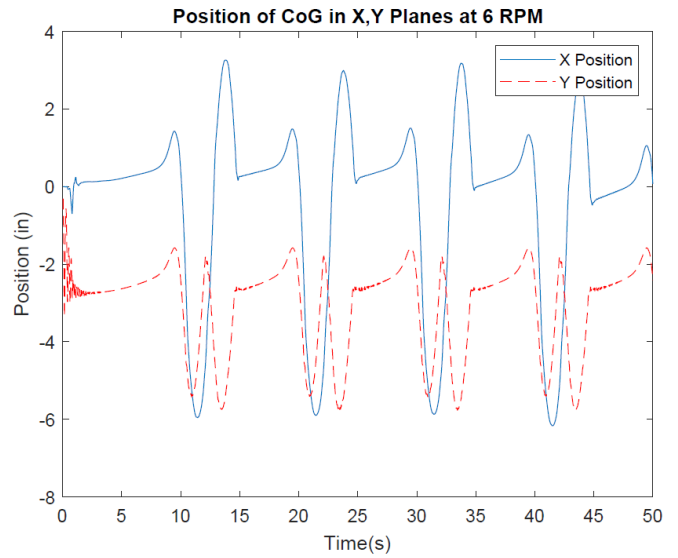


(d) X,Y planes at 10 RPM.

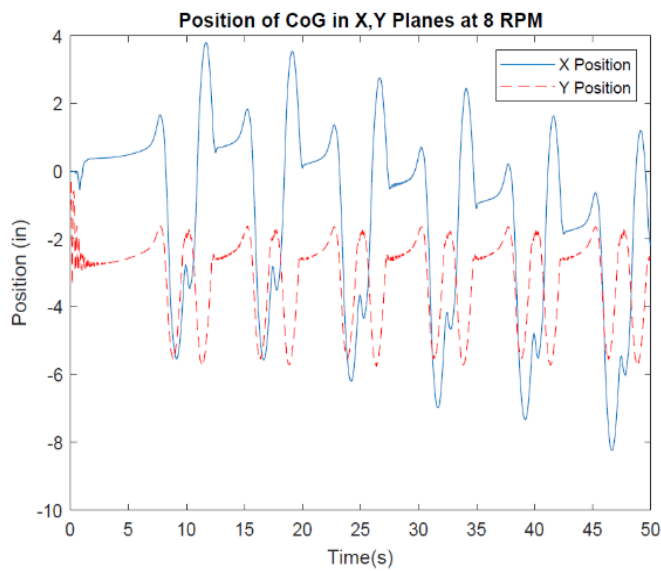
Figure 6. Acceleration of CoG for the diagonal gait.



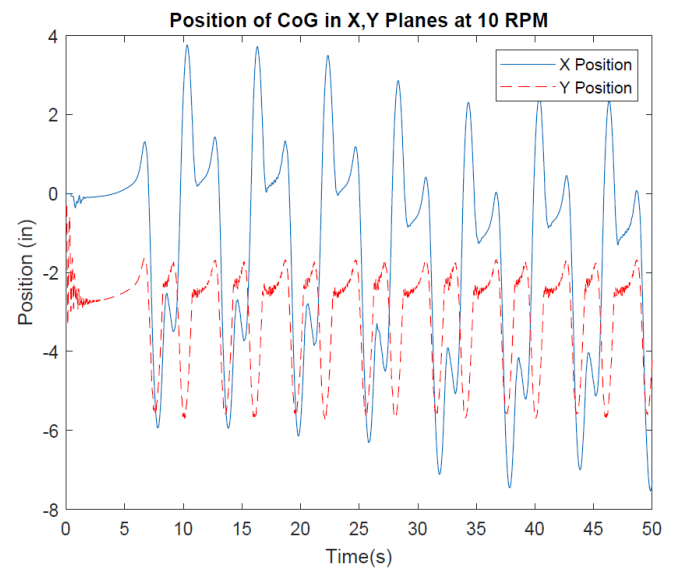
(a) X,Y planes at 4 RPM.



(b) X,Y planes at 6 RPM.



(c) X,Y planes at 8 RPM.

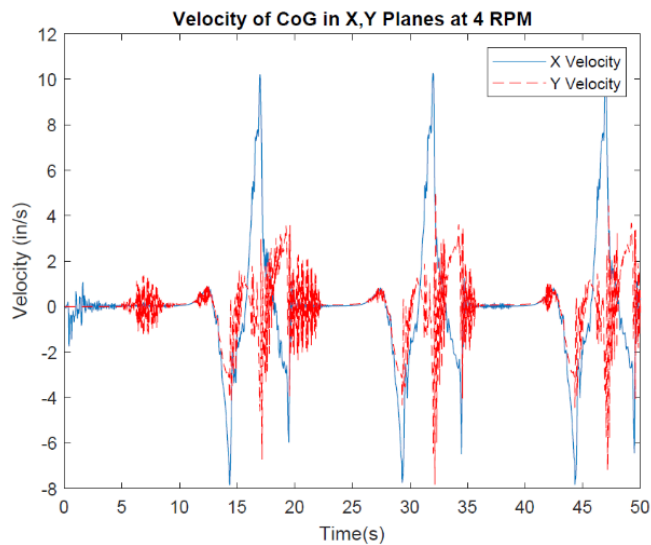


(d) X,Y planes at 10 RPM.

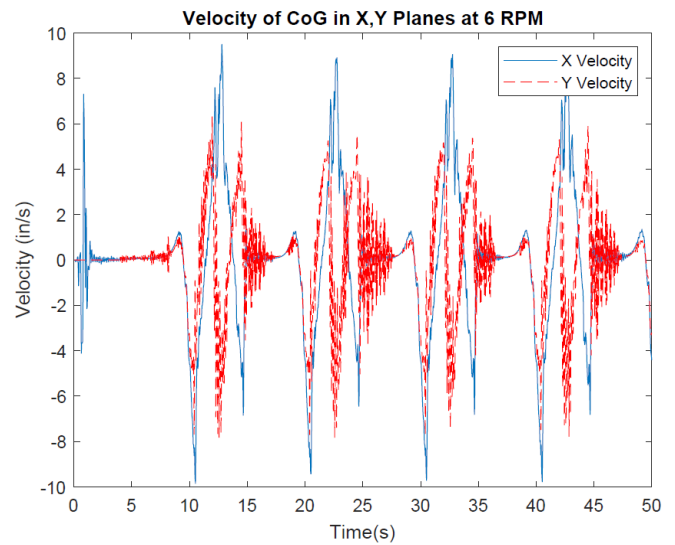
Figure 7. Position of CoG for the side gait.

Figure 8 shows the velocity in both the X and Y directions for the position of the CoG at four different rotation rates for the side gait. Figure 9 shows the acceleration in both the X and Y directions for the position of the CoG at four different rotation rates for the side gait. One of the most notable features about the side gait was its consistency across different speeds. The shape of the graphs between different RPMs are very much alike with only the period lengths decreasing and maximum values increasing for velocity and acceleration.

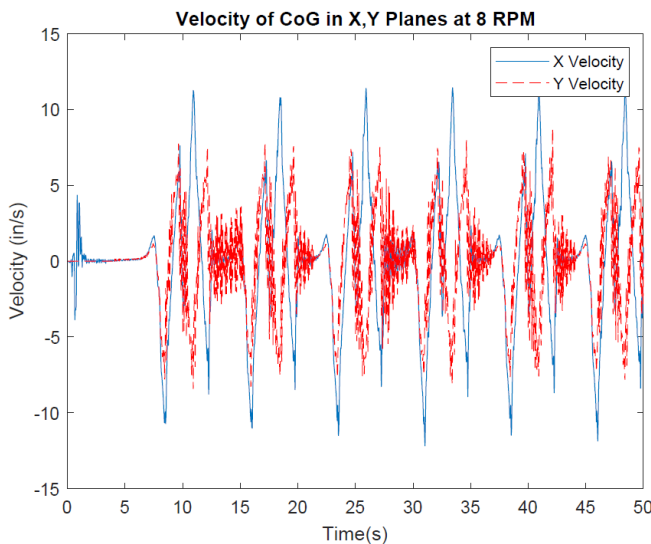
Velocity and acceleration followed the same pattern as position and have very similar graphs between the different RPMs. The velocity graph does show an increase of maximum velocities in the X direction between the graphs from 10.21 in/s for the 4 RPM graph to 13.25 in/s for the 10 RPM graph. The acceleration graphs show a max acceleration of 317.5 in/s<sup>2</sup> (0.82Gs) for 4 RPM up to 624.7 in/s<sup>2</sup> (1.6Gs) for 10 RPM in the Y direction with there being relatively insignificant acceleration in the X direction.



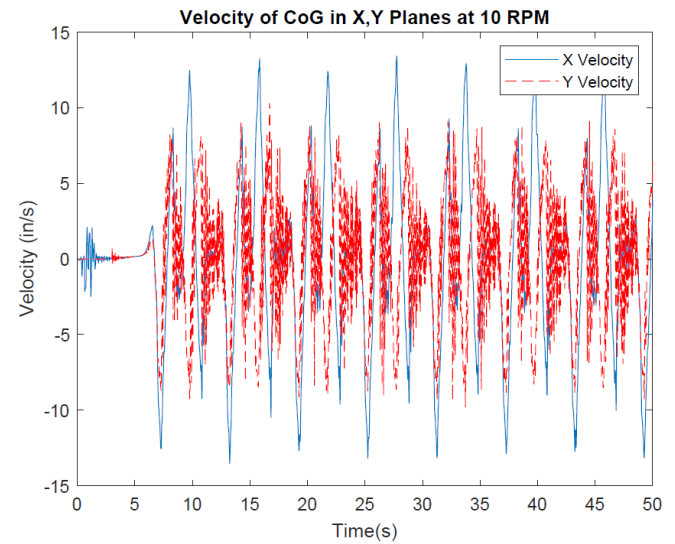
(a) X,Y planes at 4 RPM.



(b) X,Y planes at 6 RPM.

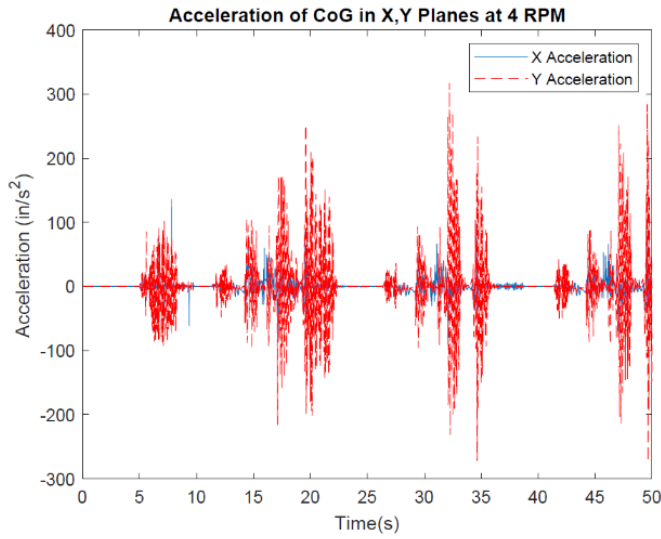


(c) X,Y planes at 8 RPM.

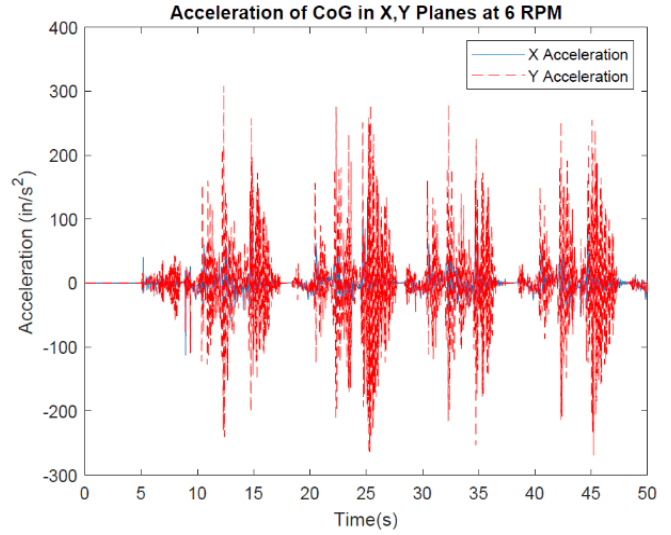


(d) X,Y planes at 10 RPM.

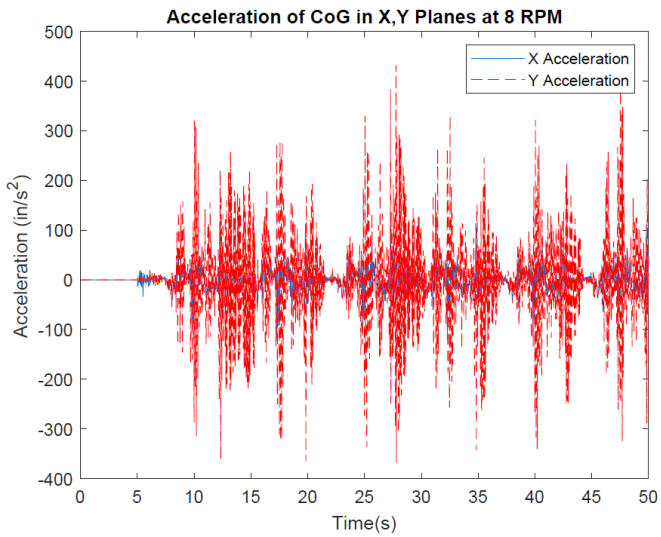
Figure 8. Velocity of CoG for the side gait.



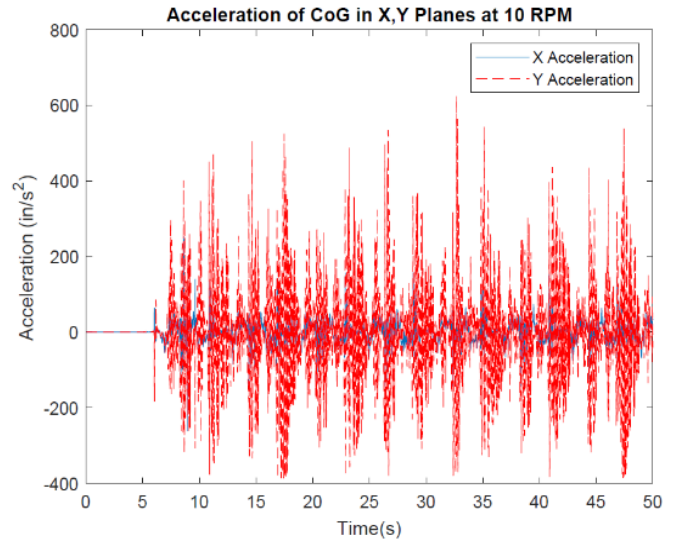
(a) X,Y planes at 4 RPM.



(b) X,Y planes at 6 RPM.



(c) X,Y planes at 8 RPM.



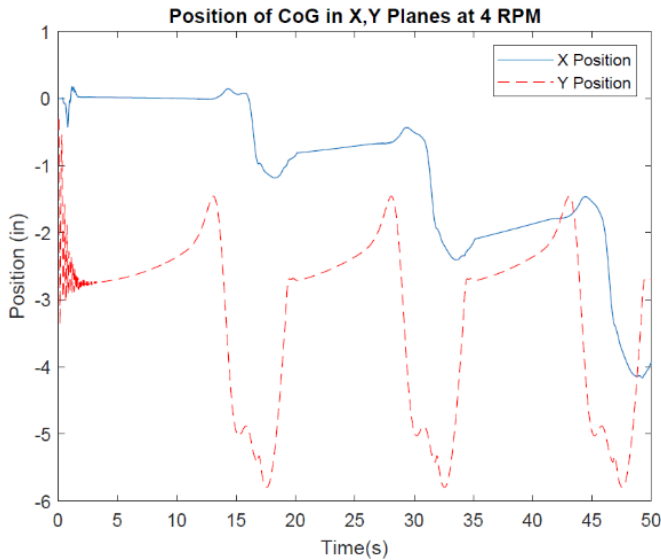
(d) X,Y planes at 10 RPM.

Figure 9. Acceleration of CoG for the side gait.

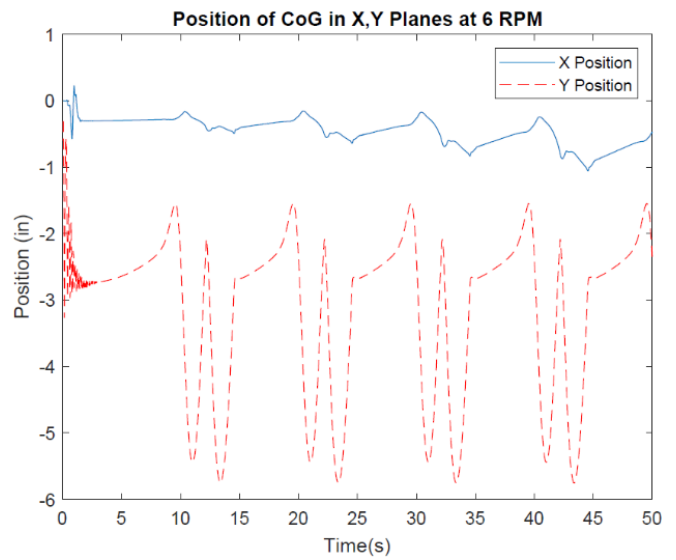


Figure 10 shows the position in both the X and Y directions for the front-back gait. The position graphs do have a piece of interesting data in that for most of the RPMs, the robot tended to stay straight or drift very slightly to the right, except for the 4 RPM graph, where the robot drifted significantly to the left. Other than that, all the position graphs have a similar distance of motion for the center of

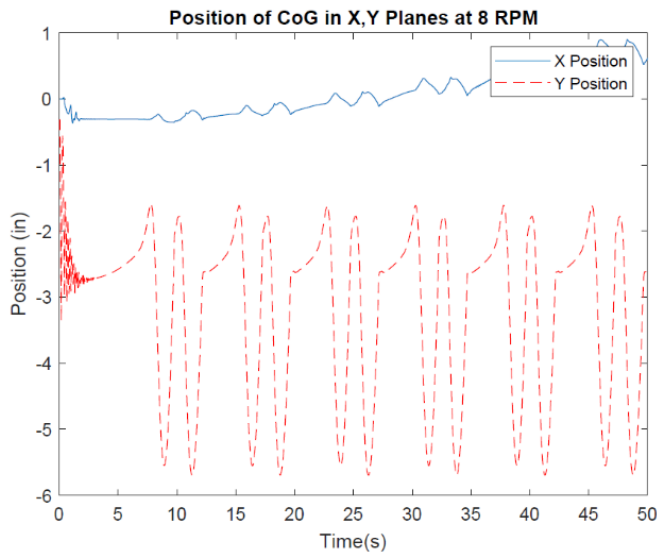
gravity in the Y direction with the average being around 4" for all the graphs. Figure 11 shows the velocity in both the X and Y directions for the position of the CoG at four different rotation rates for the front-back gait. Figure 12 shows the acceleration in both the X and Y directions for the position of the CoG at four different rotation rates for the front-back gait.



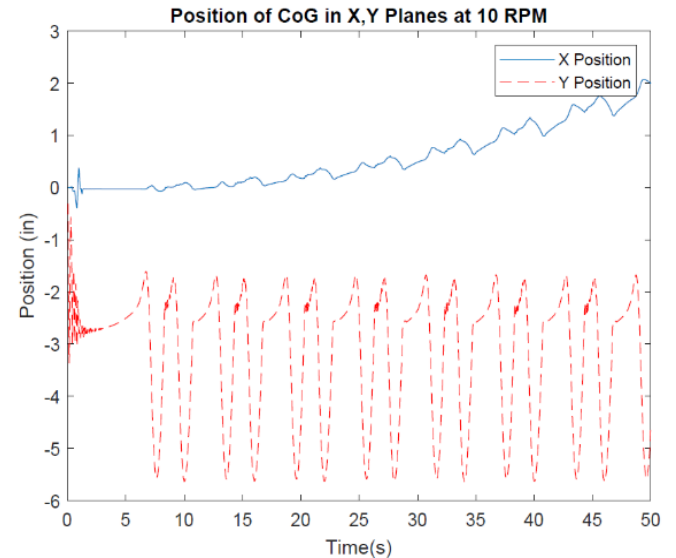
(a) X,Y planes at 4 RPM.



(b) X,Y planes at 6 RPM.

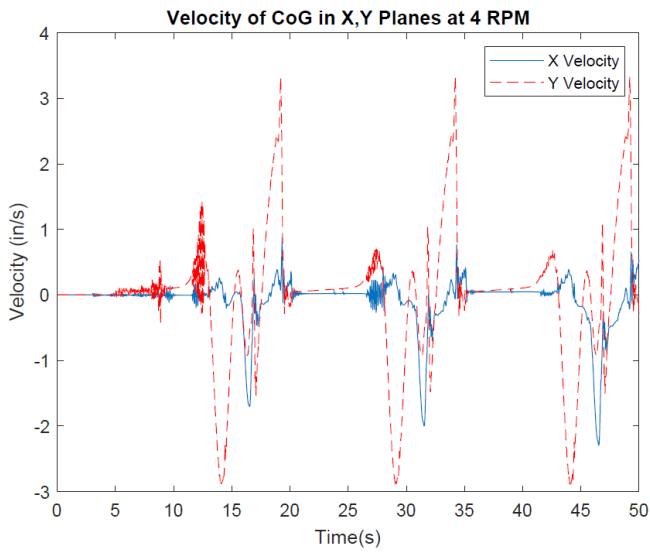


(c) X,Y planes at 8 RPM.

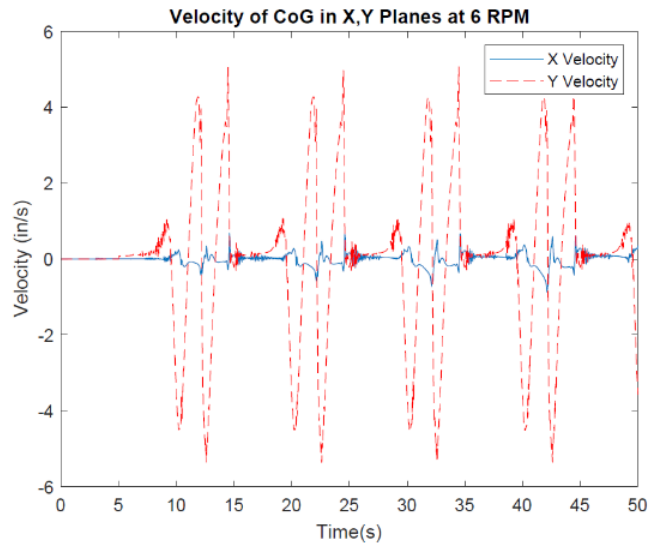


(d) X,Y planes at 10 RPM.

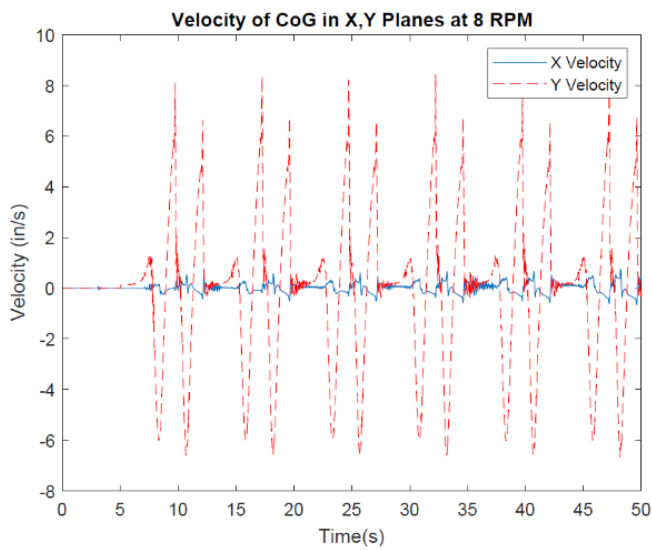
Figure 10. Position of CoG for the front-back gait.



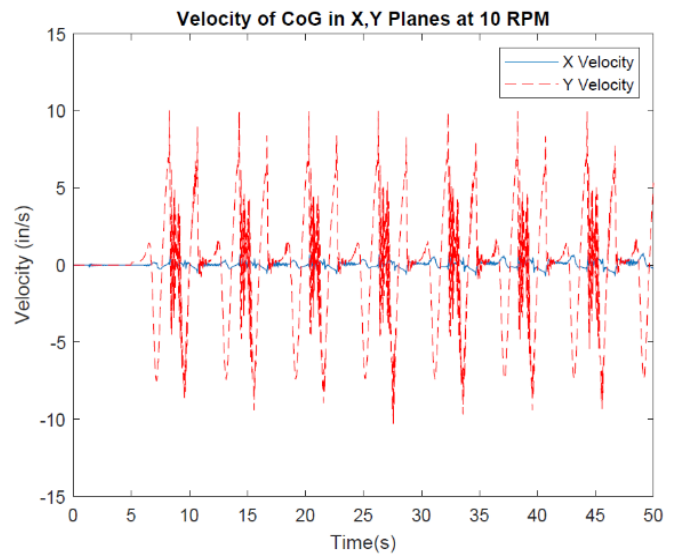
(a) X,Y planes at 4 RPM.



(b) X,Y planes at 6 RPM.



(c) X,Y planes at 8 RPM.



(d) X,Y planes at 10 RPM.

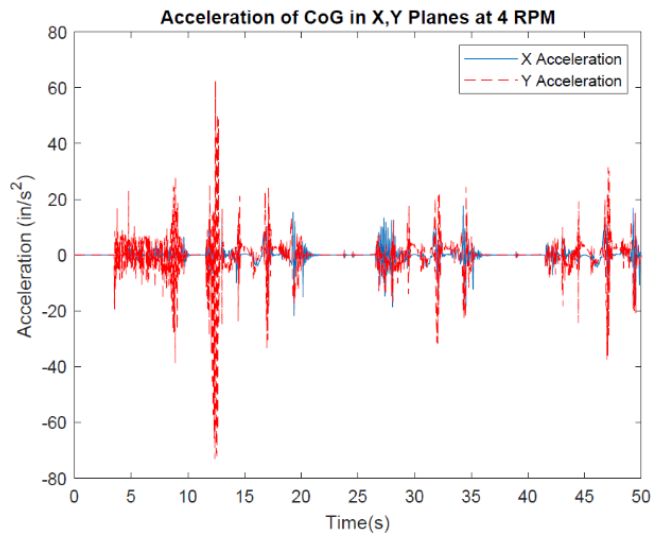
Figure 11. Velocity of CoG for the front-back gait.

The graphs for the front-back gait show the same kinds of consistency as the side gait graphs, except that in this case it is in the Y direction instead of the X. The velocity and acceleration in the X direction were extremely small, in this case with the largest X direction velocity being 2 in/s in the 4 RPM graph and the largest X direction acceleration being around 35 in/s<sup>2</sup> in the 10 RPM graph. The velocity graphs follow a pattern of decreasing periods with an increasing maximum value as RPM increases, going from 3.32 in/s at 4 RPM to 10 in/s at 10 RPM. The acceleration graphs display similar patterns with large spikes and then a period of dissi-

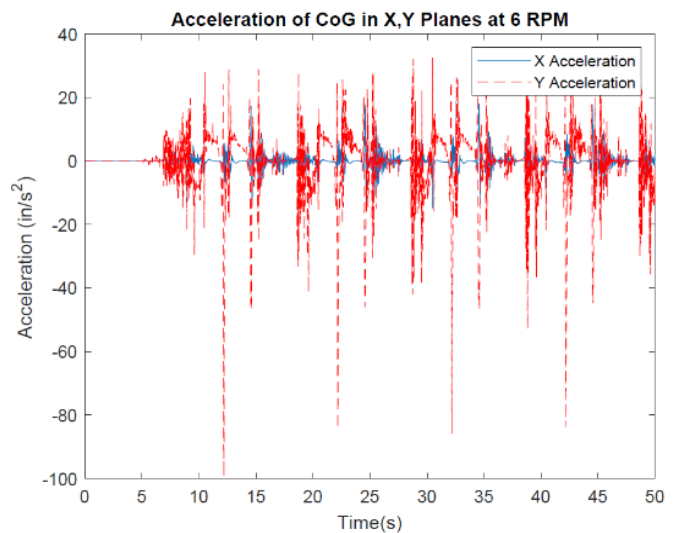
pation. The major difference is that in the 4 RPM graph there is a large spike in acceleration that is much greater than the others and is not repeated.

## Discussion

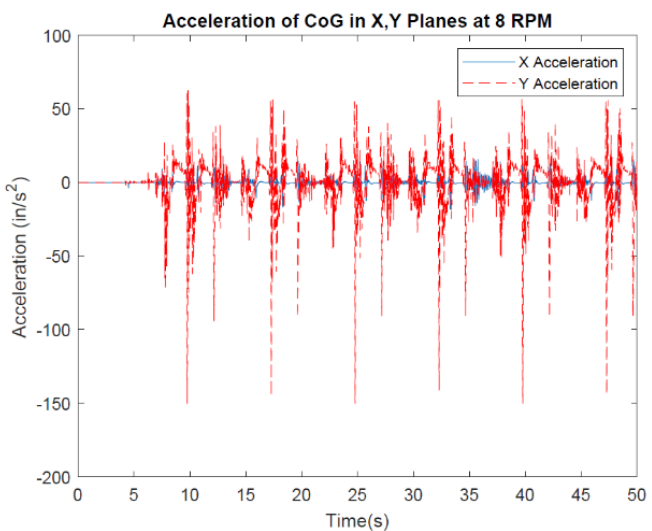
In the diagonal gait, most of the motion in the robot was in the X direction from left to right. This means that the robot was not well balanced when it was on two legs. The cause seemed to be the small loop at the end of the trajec-



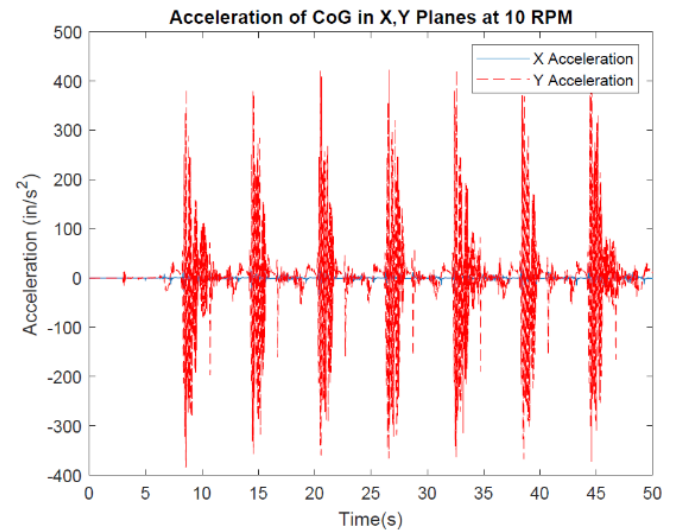
(a) X,Y planes at 4 RPM.



(b) X,Y planes at 6 RPM.



(c) X,Y planes at 8 RPM.



(d) X,Y planes at 10 RPM.

Figure 12. Acceleration of CoG for the front-back gait.

ry of the foot (Peters & Chen, 2014) causing the robot to shove itself forward before picking up its feet, thereby causing it to be off balance as the feet lifted. The drift to the left seemed to be caused by the timing of the rotation of the cams. Right after the robot shoved itself forward was when the first pair of legs rose to walk. As the second pair of legs moved to rise, they also performed this slight shoving motion. But, while the first pair of feet were just above the platform, they were shoved forward by this motion and simply hit the ground, which left the first pair of feet slightly to the left but not pitched forward, thereby providing a more stable base to balance on while the second pair of feet were in the air. Since the robot was balanced better while the second pair of feet were in the air, it also meant that they traveled in more of a straight line instead of causing the robot to lean slightly right to “correct” the trajectory of the robot. The motion in the Y direction was mostly from the actuation of the legs and the dip that the robot took from being off balance. This type of motion was acceptable and will be improved further when the robot’s balance is improved.

When examining the velocities, the velocity in the X direction was still much higher than desired but it was to be expected with the balance issues with the diagonal gait. The velocity in the Y direction also acted mostly as expected, meaning that as the RPMs, and therefore the speed, at which the leg actuated increased the velocity of the center of gravity, since it was moving up and down faster as the robot walked, but there was very little to no difference between the velocities at 8 RPM and 10 RPM. The accelerations acted as expected and desired, since the acceleration in the Y direction was much greater than the X direction, so much so that it was difficult to see the X acceleration line on the graph. Most of the g force that the robot experienced was in the direction in which it was most supported.

With the side gait, the position graph was as expected, with the X direction having the most amount of motion. Since one side tried to lift completely off the ground, the robot tipped completely that way before correcting itself, since there is no real way for it to balance. This motion of the gait could also be described as “swaying.” The velocity graph also shows the X velocity to be greater than the Y, but the acceleration in the Y direction was still greater than the X. The front-back gait, while being the most stable in the X direction, had much more motion in the Y direction than both the diagonal and side gaits. It acted similarly to the side gait in the fact that the exaggerated motion was due to the robot having no way to balance when either the front or back feet were rising, so it would fall onto them until the legs moved back into more of a straight position and the robot corrected itself. The front-back gait had an interesting acceleration chart in that it was the only one having similar 4 RPM and 6 RPM accelerations; but, as the robot operated with 8 or 10 RPM, the acceleration increased greatly. This was more in line with the idea that as the RPMs increased, so would the acceleration of the center of gravity.

## Conclusions

This work showed that a robot using single-degree-of-freedom legs can walk and stand by itself with a simple control system. However, the design was not very efficient, due to balance issues. More complex simulations are needed to optimize the placement and timing of the legs to make the robot walk effectively. Furthermore, additional simulations should address the limitations inherent in this simulation, the most significant of which is the effect of discrete timesteps, which impacts all simulations of continuous systems.

The diagonal gait was the most promising configuration out of the three gaits that were simulated. While it continued to have balance issues that need to be corrected, the other gaits underperformed to the extent that they would not warrant subsequent investigation. The side gait swayed too much from left to right, which caused issues when trying to travel on terrain that was not perfectly straight. The front-back gait had the same issues—that is that it swayed back and forth too much for it to be useful with a single-degree-of-freedom system. A robot using single-degree-of-freedom legs cannot shift its weight on its own, due to the restrictions of the design itself and the relatively simple control system to allow it to balance out the weights and use the side or front-back gait. The diagonal gait could be corrected by moving the mounting position of the cams of the legs to the main body so that they are balanced around this shoved-forward position that the trajectory of the foot imposes on the robot. Future work could be done with more sophisticated control systems that control the rotation of the cams more precisely, allowing the robot to mimic the motion of a quadrupedal animal. Another avenue for progress is to change the system from quadrupedal to a hexapod. This would always allow the robot to keep three points of contact with the ground and greatly improve the balance of the robot.

## References

- Asci, S., & Zhang, K. (2021). Design and kinematic simulation of a novel leg mechanism for multi-legged robots. *Proceedings of the International Design Engineering Technical Conferences and Computers and Information in Engineering Conference, 85451, V08BT08A023*. American Society of Mechanical Engineers.
- Buehler, M., Koditschek, D. E., & Saranli, U. (2002). *Single actuator per leg robotic hexapod*. U.S. Patent 6,481,513. Washington, DC: U.S. Patent and Trademark Office.
- Cho, J., & Kong, K. (2020). Mechanism design of a robotic leg for running considering radial force producibility and tangential mobility. *International Journal of Control, Automation and Systems, 18(7)*, 1782-1791.
- Collins, S. H., & Ruina, A. (2005). A bipedal walking robot with efficient and human-like gait. *Proceedings of the 2005 IEEE International Conference on Robotics and*

- Automation*, 1983-1988. Barcelona, Spain. IEEE.
- Fukuoka, Y., & Kimura, H. (2009). Dynamic locomotion of a biomorphic quadruped 'Tekken' robot using various gaits: walk, trot, free-gait and bound. *Applied Bionics and Biomechanics*, 6(1), 63-71.
- García-López, M. C., Gorrostieta-Hurtado, E., Vargas-Soto, E., Ramos-Arreguín, J. M., Sotomayor-Olmedo, A., & Moya Morales, J. C. (2012). Kinematic analysis for trajectory generation in one leg of a hexapod robot. *Procedia Technology*, 3, 342-350.
- Ha, S., Han, Y., & Hahn, H. (2007). Adaptive gait pattern generation of biped robot based on human's gait pattern analysis. *International Journal of Mechanical Systems Science and Engineering*, 1(2), 80-85.
- Herrero, D., & Martinez, H. (2007). Embedded behavioral control of four-legged robots. In P. Lima (Ed.), *Robotic Soccer* (chapter 11). IntechOpen. <https://doi:10.5772/49>. ISBN: 978-3-902613-21-9.
- Inagaki, S., Yuasa, H., Suzuki, T., & Arai, T. (2006). Wave CPG model for autonomous decentralized multi-legged robot: Gait generation and walking speed control. *Robotics and Autonomous Systems*, 54(2), 118-126.
- Jin, B. (2015). *Modeling of a cam-actuated robotic leg*. (Undergraduate thesis). Kettering University, Flint, MI.
- Joze, H. R. V., Habibi, J., & Asadi, N. (2007). *Impossible: A fully autonomous four-legged robot soccer team*, Robotic Soccer, Pedro Lima, ed., IntechOpen.
- Koushik, M. J., Krishna, M. A., Rahul, R., & Sreedharan, P. (2021). Foot trajectory analysis of a robotic leg. *Journal of Physics: Conference Series*, 2070(1), 1-12.
- Koutsoukis, K., & Papadopoulos, E. (2021). On the effect of robotic leg design on energy efficiency. *Proceedings of the 2021 IEEE International Conference on Robotics and Automation*, 9905-9911. Xi'an, China. IEEE.
- Kurz, M. J., Judkins, T. N., Arellano, C., & Scott-Pandorf, M. (2008). A passive dynamic walking robot that has a deterministic nonlinear gait. *Journal of Biomechanics*, 41(6), 1310-1316.
- Lewis, M. A., & Bekey, G. A. (2002). Gait adaptation in a quadruped robot. *Autonomous Robots*, 12(3), 301-312.
- Liu, Y., & Ben-Tzvi, P. (2020). An articulated closed kinematic chain planar robotic leg for high-speed locomotion. *Journal of Mechanisms and Robotics*, 12(4), 1-15.
- Nagakubo, A., & Hirose, S. (1994). Walking and running of the quadruped wall-climbing robot. *Proceedings of the 1994 IEEE International Conference on Robotics and Automation*, 1005-1012. San Diego, CA. IEEE.
- Peters, D. L., & Chen, S. (2014). Design of a cam-actuated robotic leg. *Proceedings of the International Mechanical Engineering Congress & Exhibition*, 46606, V011T14A035. American Society of Mechanical Engineers. Montreal, Canada.
- Poulakakis, I., Smith, J. A., & Buehler, M. (2005). Modeling and experiments of untethered quadrupedal running with a bounding gait: The Scout II robot. *The International Journal of Robotics Research*, 24(4), 239-256.
- Raibert, M. H. (1986). *Legged Robots That Balance*. MIT Press.
- Raibert, M., Blankespoor, K., Nelson, G., & Playter, R. (2008). Bigdog, the rough-terrain quadruped robot. *Proceedings of the 17th World Congress - The International Federation of Automatic Control*, 41(2), 10822-10825. Seoul, South Korea.
- Song, S. M., & Waldron, K. J. (1989). *Machines that walk: the adaptive suspension vehicle*. MIT press.
- Spröwitz, A., Tuleu, A., Vespignani, M., Ajallooeian, M., Badri, E., & Ijspeert, A. J. (2013). Towards dynamic trot gait locomotion: Design, control, and experiments with Cheetah-cub, a compliant quadruped robot. *The International Journal of Robotics Research*, 32(8), 932-950.
- Talebi, S., Poulakakis, I., Papadopoulos, E., & Buehler, M. (2001). Quadruped robot running with a bounding gait. In D. Rus and S. Singh (Eds.), *Experimental Robotics VII. Lecture Notes in Control and Information Sciences*, 271. Springer, Berlin, Heidelberg.
- Tsujita, K., Tsuchiya, K., & Onat, A. (2001). Adaptive gait pattern control of a quadruped locomotion robot. *Proceedings of the 2001 IEEE/RSJ International Conference on Intelligent Robots and Systems. Expanding the Societal Role of Robotics in the Next Millennium*, 4, 2318-2325. Cat. No. 01CH37180. IEEE. Maui, HI.
- Zhang, J., Gao, F., Han, X., Chen, X., & Han, X. (2014). Trot gait design and CPG method for a quadruped robot. *Journal of Bionic Engineering*, 11(1), 18-25.
- Zhang, G., Rong, X., Hui, C., Li, Y., & Li, B. (2016). Torso motion control and toe trajectory generation of a trotting quadruped robot based on virtual model control. *Advanced Robotics*, 30(4), 284-297.

## Biographies

**ANDREW J. WASSON** earned his BS in Mechanical Engineering from Kettering University in 2020. Mr. Wasson may be reached at [wass1286@kettering.edu](mailto:wass1286@kettering.edu)

**DIANE L. PETERS** is an associate professor of mechanical engineering at Kettering University. She earned her BS in Mechanical Engineering from the University of Notre Dame in 1993, MS in Mechanical Engineering in 2000 from the University of Illinois—Chicago, and PhD in Mechanical Engineering in 2010 from the University of Michigan. Dr. Peters' research interests include control co-design, control systems, and autonomous vehicles. Dr. Peters may be reached at [dpeters@kettering.edu](mailto:dpeters@kettering.edu)

**YAOMIN DONG** is currently a Professor of Mechanical Engineering at Kettering University. He received his PhD in Mechanical Engineering from the University of Kentucky in 1998. Dr. Dong has extensive R&D experience in the automotive industry and holds multiple patents. Dr. Dong's areas of expertise include metal-forming processes, design with composite materials, computer graphics, computer-aided engineering, and finite element analysis. Dr. Dong may be reached at [ydong@kettering.edu](mailto:ydong@kettering.edu)

# AUTOMATED WATER BOTTLE PACKAGING SYSTEM

Maged Mikhail, Purdue University Northwest; Mateusz Plachta, Purdue University Northwest;  
Adalberto Acosta, Purdue University Northwest

## Abstract

With the rise of variability in manufacturing, the necessity for flexibility in automation is increasing in significance. Be it with small or large companies, it is important to be able to save resources where possible and eliminate costs for things that quickly become obsolete on the assembly line. With the improvements in robotics technology, it has become simpler to use robots with specialized attachments and replace dedicated assembly machinery in manufacturing settings. The goal of this study was to demonstrate the efficacy of replacing current superfluous, expensive machinery with robotic arms via the design and assembly of an automated water bottle packaging system that uses devices and materials found on site. In this paper, the authors detail project goals, specifications, and deliverables, as well as the complete design of the system. Also presented are the calculations and testing procedures used for the project design and details of the project schedule and budget.

## Introduction

The purpose of this project was to provide a conceptual framework of how a robotic arm can be used to replace the necessity for dedicated machinery in packaging warehouses. In this paper, the authors provide measurable goals and specifications, project deliverables, methodology, theoretical background, design, chronological outline, and costs for the design. During the initial phases of the robot's programming, it was able to pick up a box that would then be filled with bottles, sealed within the box, and returned to the starting point. This would usually take a three-step process involving a lengthy conveyor track, a bottle placing unit, and a box packaging machine. This all would take an excessive amount of space and resources to accomplish, when compared to the simpler costs of a single robot that, in a changing environment, can be flexible enough to change with it.

## Project Goals

The creation of this robotic packaging line had the following goals.

- Create an efficient water bottle packaging system
- Easily pick-and-place bottles for packaging
- Efficiently fold lids and seal boxes
- Control and monitor the system using an HMI panel
- Develop a packaging system that allows easy maintenance.

## Specifications

- The HMI display will control the packaging system via virtual "START" and "STOP" buttons, as well as determine the number of packaged bottles and sealed boxes.
- Water bottles with a height of 4" and a diameter of 2.5" are placed at the starting point of the primary conveyor belt system manually.
- The bottle conveyor system will run at a constant speed of 6.6 bottles/min.
- An 8" x 8" x 5" cardboard box will be placed at the starting point of a secondary conveyor belt system.
- An optic/proximity sensor located at the end of the bottle-transporting conveyor belt and the box-transporting belt will be calibrated to detect an object at 0.5" from itself.
- A Fanuc robot will operate at a maximum speed of 225 mm/s.
- The robot will place nine bottles into the box before proceeding to the lid-folding and sealing step.
- Three-inch strips of double-sided tape will be placed onto the cardboard box flaps before placing them onto the conveyor.
- The pressure used for the pneumatic system is kept at 40 psi.
- The entire water bottle packaging cycle takes no more than four minutes to complete.

## Deliverables

The deliverables of the project include:

- CAD models and drawings
- Calculations and analysis
- A project schedules
- A project budgets
- Testing data
- A completely built packaging system
- Risk assessment
- PLC programming
- Fanuc robot programming

## Methodology

The design of the automated water bottle packaging system was completed with concepts taken from Advanced Instrumentation and Automation for Filling and Packaging of Beverages (Development of an Educational Robot Vision System, 2012; Chatterjee, 2014). Figure 1 shows the calcu-

lations used to determine the total travel distance of the Fanuc robot during the bottle packaging process for one cycle, based on a simulated system created in SolidWorks. These travel-distance calculations helped determine an appropriate speed for bottle transportation via a conveyor line. Calculations were also used to determine the total power consumption of the electrical components within the system, which were based on real-time measurements. Access to the equipment and machinery was granted by the technology department of Purdue University Northwest. Testing was conducted in steps during the assembly and programming phases to confirm the proper functioning of all electro-mechanical and pneumatic devices (Mikhail & Wang, 2020). Due to the low cost of required components and materials, the project was funded by project group members.

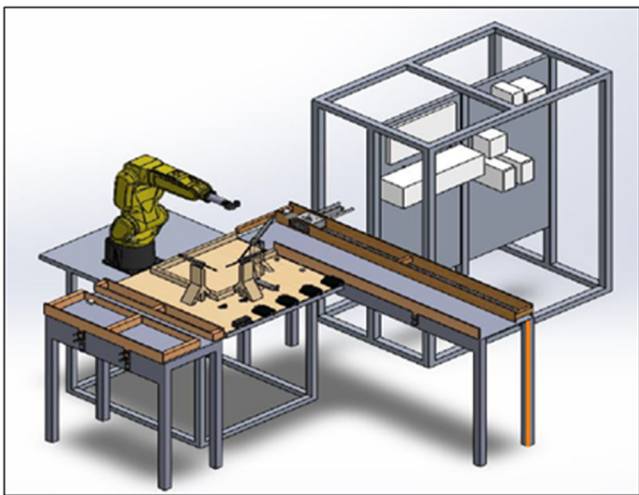


Figure 1. Complete system assembly model.

Each subassembly was a separate part of the packaging system with some interconnected components, such as the electrical and communication wiring between the robot and the Allen-Bradley trainer (Kwak & Mikhail, 2020).

## Robot Work Cell Assembly

The robot work cell assembly consisted of an aluminum table and a Fanuc LRMate 200iD/4S 6-axis robot. The aluminum table was a pre-built model with a length of 44", a width of 27.5", and a height of 35". The tabletop, with a thickness of 1.25", had 13 half-inch diameter holes on each side, spaced one inch apart. The holes were placed 1.25" from the edges of the table. The tabletop was used for mounting the robot as well as the custom packaging base, and acted as the work envelope of the packaging procedure. Figure 2 shows how the Fanuc robot was mounted onto the tabletop at a fixed position. The robot was placed about 5" from the left side and 9.5" from the back of the table. The robot was connected to its controller and teach pendant, which was placed underneath the tabletop. The robot was

used to execute the packaging operations via pick-and-place and point-to-point motions.

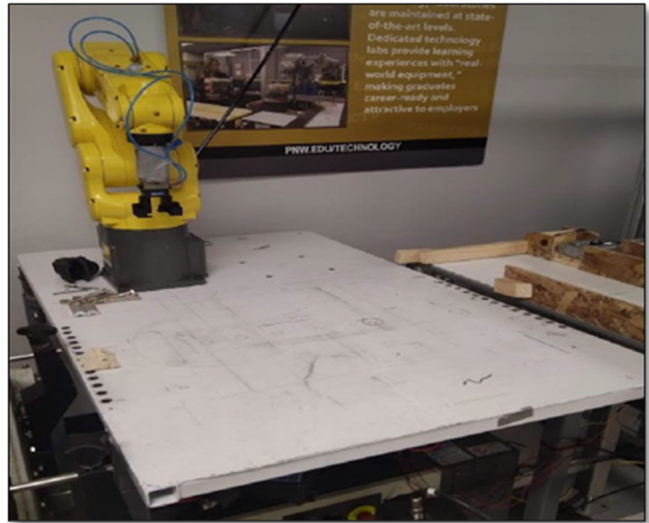


Figure 2. Fanuc LR Mate 200 iD/4S robot on an aluminum table.

A custom 3D-printed gripper was attached to the pneumatic end tool located at the end of the robotic arm. Figure 3 shows the gripper composed of two mirrored jaw pieces with a large slot in front when assembled. The jaws of the gripper were designed to fit a one-inch-diameter cap of a standard 8 FL OZ water bottle. There was a small shelf at the bottom of the slot on both sides of the jaws to allow the bottle cap's lower ring to hook on when the gripper was closed.

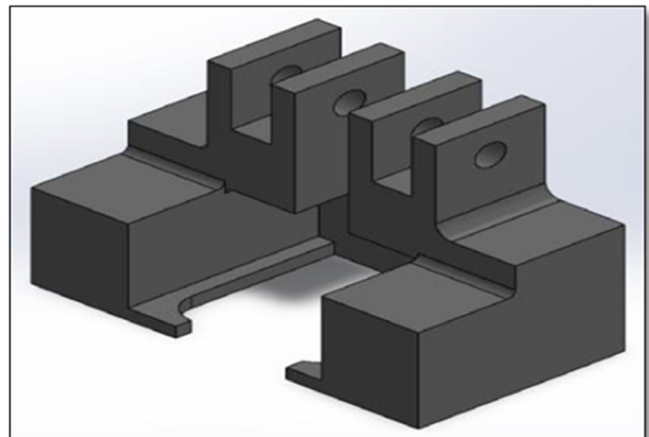


Figure 3. Custom gripper model.

The robot used the gripper to direct a packaging box to and from the box conveyor line and across the packaging base as well as pick up the appropriate water bottles by the cap from the bottle conveyor line and then insert them into the packaged box. The gripper was also used to press and hold down the remaining back flap of the box during the lid-closing procedure.

## Custom Packaging Base Assembly

Figure 4 shows a custom base with attached pneumatic cylinders that was designed and created to serve as a packaging zone for the system. The base platform was built out of 24" x 24" x 1/2" plywood, with the walls constructed from 1 1/2" x 3/4" wood blocks. There was an 8.5-inch-wide path that led from the right side of the board to an empty, encased area that was designated to be the packaging location of the box, where it will travel to and from the box conveyor. The base pathway was designed to fit and align the packaged boxes during box movement. When a box was directed to the designated packaging zone, it would then be pressed up against the front wall. When packaging procedures were performed, the robot would shift the box through the same pathway and knot the box conveyor line located right from the base. Two 1/2-inch holes were made on the right side of the base to mount it onto the robot work cell table via 1/2-inch hex head cap bolts.

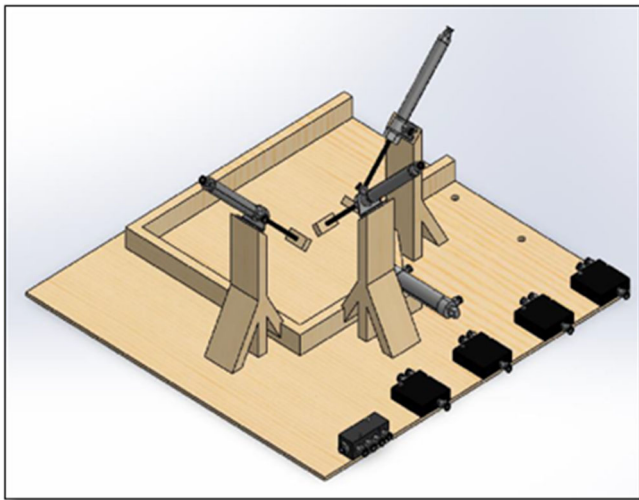


Figure 4. Pneumatic packaging base.

Three wooden support blocks were constructed and attached to the packaging slot walls with wood screws, with each one being on a different side of the packaging area. The wooden support blocks were 9.25" in height with a 45° cut facing the front. A truss was used to support the vertical block and prevent it from breaking due to excessive forces. Figure 5 shows how, at the top of the 45° surface, a Bimba four-inch-stroke, double-acting pneumatic cylinder, was mounted into a D-129-cylinder bracket and attached to the support block with wood screws. The cylinders were mounted facing downward towards the packaging zone and positioned so the rods extended towards the center of the top surface of the box during the lid-folding procedure. A PanelView Plus 1000 HMI was used to control and monitor the operations of the packaging system. The operator panel was designed in FactoryTalk View Studio and then uploaded into the physical device memory. The panel

contained controls for the operator to start and stop the packaging cycle, as well as clear the faults on all devices. There were numeric string displays to indicate the number of bottles and boxes packaged along with lights to indicate the state of the system.



Figure 5. Bimba 094-DP pneumatic cylinder.

The design of the main packaging operator panel contained the main controls of the system, the status indicator lights for system operations, and the displays for the number of packaged items. There was a panel with five control pushbuttons located on the left side of the screen. The "Clear Faults" button was used to remove any faults present on both Powerflex 525 devices and the Fanuc 6-axis robot. After clearing the faults, the "Start" button could be pressed to start the packaging system, as it began the cycle and activated the robot programming. The "Stop" and "E-Stop" buttons were used to stop the conveyor systems and robot. The "Reset Count" button reset the number of packaged bottles and boxes.

In the center of the screen was a panel indicating system operations in which six indicator lights and two numeric displays were present. The six lights corresponded to the labeled system states and, when inactive, the lights would blink red. When the system item was active, the associated light would be green. The two numeric displays were used by the system to indicate the number of packaged items, which came from the ControlLogix PLC programming.



## Programming

The programming designed for controlling the automated water bottle packaging system was broken down into two types. The first type was the teach pendant programming created to control the Fanuc 6-axis robot, as well as change the states of its digital inputs and outputs. The other type was the PLC programming done in Studio 5000 software to control, mediate, and monitor the involved Allen-Bradley devices, as well as to communicate with the robot.

### Teach Pendant Programming

The main teach pendant programming would run when the packaging cycle was started. According to the program section in Table 1, the robot would wait in a jump-label loop until a box was detected by the sensor, which would change the state of the digital input “DI22” and allow the robot to continue.

Table 1. Robot main program.

```
1: LBL (3) ;
2: IF (DI (22) =ON) THEN;
3: JMP LBL (2);
4: ENDIF;
5: JMP LBL (3);
6: LBL (2)
```

When the robot progressed to line 6, the value of register R3 was set to zero, and the X and Y coordinate data of position register PR3 were reset. The robot then waited two seconds before traveling to the cardboard box via pick-and-place movement and then directing it to the packaging area via point-to-point movement. Table 2 shows that digital output DO30 then turned on, marking the beginning of the bottle packaging phase, and the program moved to the box packaging subroutine. The system remained in the bottle subprogram until all nine bottles were packaged.

### PLC Programming

The PLC programming created in Studio 5000 was used to control and mediate electrical signals between the devices of different subassemblies, such as the Allen-Bradley devices on the trainer panel or the solenoid valves on the pneumatic base. The PLC programming can be broken down into the main control program, box conveyor subprogram, bottle conveyor subprogram, and the CompactLogix subprogram. Table 3 shows that in the main PLC program, downloaded into the ControlLogix controller, the two control subprograms for running the conveyor systems are active for as long as the program is running.

Table 2. Robot main program 2 (Mikhail & Abad, 2021).

```
10: WAIT 2.00(sec);
11: J P [1] 50% FINE;
12: J P [2] 50% FINE;
13: L P [3] 200mm/sec FINE;
14: L P [4] 200mm/sec FINE;
15: L P [5] 200mm/sec FINE;
16: L P [6] 200mm/sec FINE;
17: L P [7] 200mm/sec FINE
18: L P [8] 200mm/sec FINE
19: L P [9] 150mm/sec FINE
20: J P [11] 50% FINE;
21: J P [7] 50% FINE;
22: DO [30] =ON;
23: LBL [1];
24: CALL AWP;
25: IF R [3] <=2, JMP LBL [1];
```

Table 3. Structured text PLC main program.

```
if Vk_RobotStart OR Run And Not VK_RobotStop then;
Run: =1;
fanuc:O.Data[0].0:=1;
fanuc:O.Data[0].1 :=1;
fanuc:O.Data[0].2: =1;
fanuc:O.Data[0].7: =1;
TONR(T1_ST);
T1_ST.Reset: =0;
T1_ST.TimerEnable: =1;
T1_ST.PRE: =1000;
fanuc:O.Data[0].7: =T1_ST.TT;
TOFR(T2_ST);
T2_ST.Reset: =0;
T2_ST.TimerEnable:=1;
T2_ST.PRE: =1000;
fanuc:O.Data[0].5: =T2_ST.TT;
else
Run: =0;
fanuc:O.Data[0].0: =0;
fanuc:O.Data[0].1: =0;
fanuc:O.Data[0].2: =0;
fanuc:O.Data[0].7: =0;
```

Table 4. Test results, problems, and solutions.

Test	#	Results	Problems	Remedies
Bottle Conveyor Control and Movement	6	Conveyor line runs smoothly Full control of conveyor starts and stops Adjusted speed appropriate for transportation Bottles do not fall over	None	None
Box Conveyor Control and Movement	4	Conveyor line runs smoothly	Low-speed application	Powerflex frequency increased to 2000 for speed gain
Sensor and Solenoid Valve Produced- Consumed Tags	9	Full control of conveyor starts stops, and bi-directional motion	None	None
Bottle Packaging Subroutine	17	Initial speed too slow for the application	Air tubes on the robot arm side drag onto the flap of the box, causing additional tilting	Air tubes are taped down to the arm of the robot

## Testing

Preliminary tests were done on-site to test the proper functioning of some of the individual system components. First, the conveyor system motor power cables were wired to the variable frequency drives, and then the Allen-Bradley trainer was turned on. Table 4 shows that after setting up the communication modules, a simple program for controlling the VFD outputs was created in Studio 5000, which was then downloaded into the 1756-L75 ControlLogix PLC. The program was activated, and then individual virtual inputs were toggled to momentarily energize the “clear faults,” “start,” “stop,” “forward,” and “reverse” VFD outputs. A move function was also used to send a value of 350 to the frequency command output of the VFD to adjust the speed of the motors. Table 4 summarizes the results of the tests, the problems observed that resulted from them, and the actions taken to eliminate or mitigate the issues.

Additional minor tests were conducted to verify the other operations of the packaging system, such as box lid folding and sealing, box transportation to and from the box conveyor line, and the operations of the HMI panel. Figure 6 shows that, for the box-folding application, boxes with unfolded lids were placed into the packaging zone and the cylinder rods were triggered to extend, thus observing if the lid could be closed properly by the pistons. As for the box transportation test, an empty and a full box were placed inside the pathway and the robot was briefly programmed to direct both boxes between the packaging area and the box conveyor line entrance point. The fully automated water bottle packaging system was tested and validated after all modifications were completed. Figure 7 shows the complete setup (Gretsch, 2014).

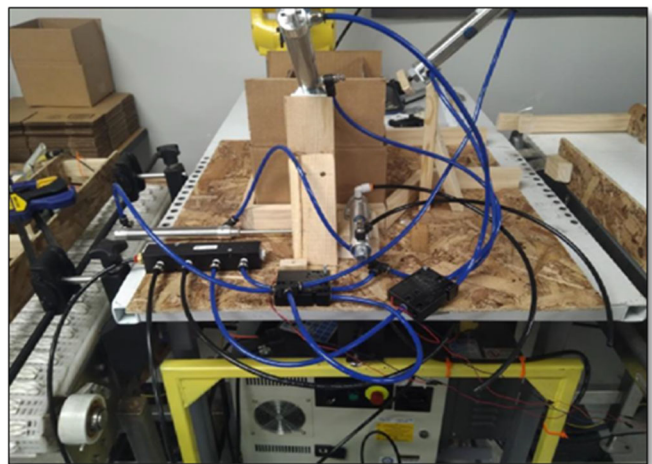


Figure 6. Packaging cycle testing preparations.

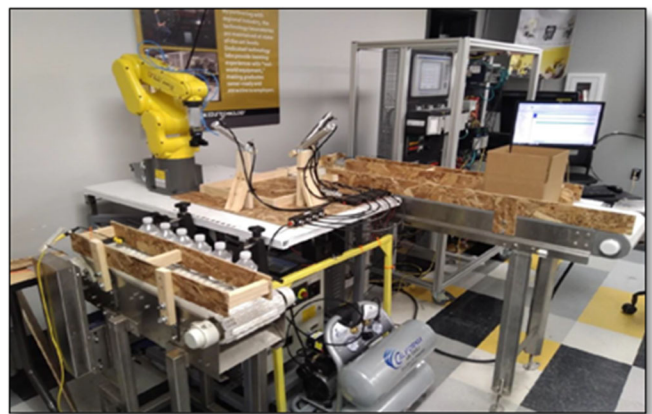


Figure 7. Automated water bottle packaging system.

## Calculations

The packaging time of the robot was then calculated by using the total sum of the travel distance taken by the gripper and the maximum robot speed in each mode, which was 225 mm/sec, and inserting both into the velocity defined by Equation 1:

$$S_t = S_o + 18S_p + 18S_D + 2\sum S_{a(1-9)} \quad (1)$$

where,

$S_t$  is the total distance the robot gripper travels for bottles.

$S_o$  is the distance from the gripper to the bottle approach point.

$S_p$  is the distance from the bottle approach point to the bottle pick-up point.

$S_D$  is the distance from the bottle placement approach point to the bottle destination point in box.

$S_a$  is the distance between the bottle approach point to each bottle and the placement point above the box.

$$S_t = 725.68''$$

The calculated time was then utilized to obtain the packaging speed of the robot in bottles-per-minute via a ratio defined by Equation 2:

$$t_B = \frac{S_t}{V_t} = 81.8 \text{ sec} \quad (2)$$

where,

$t_B$  is the bottle packaging time.

$V_t$  is the maximum robot speed in teach mode.

The speed of the bottle conveyor line was calculated with an assumed time of 60 seconds for transporting the nine water bottles. The time was divided by the number of bottles to get the time required for one bottle to be transported. The resulting time was then used to calculate the speed of the conveyor belt, where the distance was the conveyor length of 28", as defined by Equation 3:

$$V_B = \frac{S_B}{T_{SB}} \quad (3)$$

where,

$V_B$  is the bottle conveyor speed.

$S_B$  is the bottle conveyor line length (= 28").

$T_{SB}$  is the time of travel for single bottle (= 6.7 sec/bottle).

$$V_B = 4.18 \text{ in/sec}$$

## Troubleshooting and Testing

Regarding troubleshooting, there were minimal issues encountered with the initial program. However, a significant problem was identified with the LIM function blocks, which

were not functioning correctly. Fortunately, a quick online search and feedback from an instructor provided a solution. By inputting the low value into the low limit and the high value into the high limit, the function block could successfully verify if the test value was within the specified range. Conversely, if the low- and high-value inputs were swapped, with the low value assigned to the high-limit input and the high value assigned to the low-limit input, the function block would accurately determine if the test value fell outside the designated range.

## Conclusions

The results of the project indicate that the custom automated water bottle packaging system was able to package a set of nine water bottles inside a cardboard box, fold down the lid, and seal the box shut. The bottles were easily picked up by the robot using the custom 3D-printed gripper. With the use of the pneumatic system, the box lid was folded down and kept shut, despite minor issues with one of the cylinder rods. The package lid was kept shut with the use of double-sided tape, fulfilling the sealing criteria of the project. With the assistance of the pneumatic cylinders, the Fanuc robot could transport the cardboard box to and from the box conveyor belt before and after the packaging procedures. The system was able to be run and stopped by the HMI panel controls, and the indicator lights lit up according to the state of the system. It was determined that the packaging cycle took almost the full four minutes to complete, with a robot auto mode speed at 50%; thus, with a higher setting, the cycle would take less time to complete.

## References

- Chatterjee, R. (2014, March). Advanced Color Machine Vision and Applications. [https://www.visiononline.org/userAssets/aiaUploads/file/CVP\\_Advance-Color-Machine-Vision-and-Applications\\_Romik-Chatterjee.pdf](https://www.visiononline.org/userAssets/aiaUploads/file/CVP_Advance-Color-Machine-Vision-and-Applications_Romik-Chatterjee.pdf)
- Development of an Educational Robot Vision System (2012). <https://www.semanticscholar.org/paper/Development-of-an-Educational-Robot-Vision-System/0f31eee0286482f15c9e71159ffb9cde164aafc>
- Gretsch, D. L. (2014). *Occupational Safety and Health for Technologists, Engineers, and Managers* (8<sup>th</sup> ed.). New Jersey: Pearson Prentice-Hall
- Kwak, D., & Mikhail, M. (2020, March 12-15). *Verifying Industrial Robotic Applications Using Simulation Software* [Conference presentation]. IEEE Southeast Con-20, Raleigh, NC, USA. 10.1109/SoutheastCon44009.2020.9249719
- Mikhail, M., & Abad, K. (2021). Robotics Vision System Integration for Sorting and Pick and Place Applications. *International Journal of Engineering Research, and Innovation*, 21(2), 27-34. [https://tij.org/issues/issues/spring2021/X\\_TIJ%20spring%202021%20v21%20n2.pdf#page=29](https://tij.org/issues/issues/spring2021/X_TIJ%20spring%202021%20v21%20n2.pdf#page=29)

---

Mikhail, M., & Wang, S. (2020, March 12-15). *Flexible Automation Cell Integration and Application* [Conference presentation]. IEEE Southeast Con-20, Raleigh, NC, USA. <https://ieeexplore.ieee.org/document/9439009>

## Biographies

**MAGED MIKHAIL** is an associate professor and Program Coordinator of the Mechatronics Engineering Technology Program at Purdue University Northwest. He earned his BS in Cairo, Egypt, in 2001; MS in Electrical Engineering science in 2007 from Tennessee State University; and PhD in Computer Information System Engineering in 2013 from Tennessee State University. Dr. Mikhail's research interests include vision systems, robotics, and control. Dr. Mikhail may be reached at [mmikhail@PNW.edu](mailto:mmikhail@PNW.edu)

**MATEUSZ PLACHTA** is a student at Purdue University Northwest. Mr. Plachta is pursuing work in the field of mechatronics. Mr. Plachta may be reached at [mplachta@pnw.edu](mailto:mplachta@pnw.edu)

**ADALBERTO ACOSTA** is a student at Purdue University Northwest. Mr. Acosta is pursuing a BS degree in Mechatronics Engineering Technology. Mr. Acosta may be reached at [acosta27@purdue.edu](mailto:acosta27@purdue.edu)

# AUTONOMOUS AQUACULTURE WATER QUALITY MONITORING SYSTEM

Jade Chapman, Texas A&M University; Kevin Zhang, Texas A&M University; Gage Arter, Texas A&M University; Truc Le, Texas A&M University; Dr. Rainer Fink, Texas A&M University; Dr. Ben Zoghi, Texas A&M University

## Abstract

Aquaculture is one of the fastest-growing business sectors globally and is anticipated to continue to increase substantially due to the global demand for fish and shellfish. Keeping a well-maintained aquatic environment is difficult, due to the complexity of monitoring the three most common naturally occurring water contaminants: nitrite, nitrate, and ammonia. Water quality measurement is critical in all environments, including maintaining a fish tank to keep a few aquatic fish in the living room or, on a larger scale, farming fish and crustaceans for human consumption. Although every aquatic environment requires monitoring of nitrate, nitrite, and ammonia concentrations in the water, it becomes crucial for high-density aquatic farming. At night, phytoplankton and other microorganisms become inactive, resulting in an increased concentration of these three chemicals, thereby resulting in harm to the livestock. The traditional way of measuring these three elements is through test kits that rely on visual determination by paper color after chemical interaction. However, they are time-consuming, inaccurate, and messy. Having a system that checks these three levels regularly could provide a significant improvement in fish management, resulting in increased livestock size, quality, and health.

While monitoring of all chemical and environmental factors in aquaculture is important, the sole purpose of this project was to reduce the difficulty in measuring the chemicals involved in the nitrification process. The design described here documents an automated system to optically measure ammonia, nitrite, and nitrate levels in water samples in real time. The system used a color sensor and well-established chemical mixtures to determine the concentrations of each toxic nitrification by-product in an aquatic environment. The system enables the user to determine toxicity levels without the hassle of manual testing. Automation also reduces the inherent inaccuracies associated with visual inspection. With this technology, the aquaculture industry will join the Industrial Internet of Things (IIoT), becoming an automated world of measuring, filtering, and producing fish safely and more efficiently on a large-scale basis (Elsokah & Sakah, 2019).

## Introduction

With an explosively growing world population, the need for efficient, economical, and safe food production is at an all-time high. Seafood sourced from international producers has traditionally involved a significant risk of chemical

contamination due to a lack of quality control and chemical intervention when production problems arise abroad (Ertör, 2018; Lehane, 2013; Marine Fisheries & Aquaculture Series, 2002-2003). Additionally, the shipping and temperature controls required to transport products to the U.S. dramatically increase the carbon footprint required to create and distribute the final product (Goddek, Joyce, Kotzen & Burnell, 2019). Sustainable production of aquatic products within the U.S., under strict Food and Drug Authority (FDA) quality control, will result in a higher quality product, while reducing the carbon footprint required to create the product.

Seafood has slowly become considered the most efficient type of meat to produce, resulting in a push towards effective aquatic farming in recent years (Goddek et al., 2019). In any successful aquaculture environment, the water quality is of utmost importance, increasing significantly based on fish species, size, and density. Although total water quality includes chemical control as well as environmental control, the system design presented here focuses on the three direct by-products of aquatic life: ammonia, nitrite, and nitrate. While nitrogen is essential to all living organisms, as it consists of the amino acids that make up the protein needed for plant growth, the forms of nitrogen-based compounds found in the aquatic environment can be toxic if left to increase in concentration (Boyd, 2019). This toxic effect is a problem in both freshwater and saltwater environments. Two of the nitrogen-cycle by-products (ammonia and nitrite) can be controlled through bacterial processes to create the final chemical, nitrate, which can be removed using plants in a hydroponic process. In an emergency, all these chemical concentrations can be reduced through water changes.

From homeowners with fish tanks to farmers with large aquaculture farms, there is a significant problem in keeping aquatic life healthy in a cost-effective and safe way. By autonomously measuring the concentration of the chemicals produced naturally during the nitrogen cycle, a real-time monitor can reduce the manpower needed to maintain an aquaculture system, while reducing the uncertainty involved in the current visual inspection measurement process.

## Conceptual Design

To understand the automation project described here, one must understand the manual process being used today to measure the chemical concentrations in aquatic environ-

ments. As an example, using a freshwater test kit to measure the ammonia concentration in a water sample, the test kit instructions entail the following steps.

1. Fill water to the 5 ml line in the provided test tube
2. Add 5 drops of solution 1
3. Add 3 drops of test solution 2
4. Shake test tube for 5 minutes
5. Let rest for 3 minutes
6. Hold test tube next to the color chart (provided) and optically determine the color level that best matches the color of the water in the test tube.

The automation process used in this current project required the design, control, and construction of an electro-mechanical system that could complete all steps involved in the measurement of ammonia, nitrite, and nitrate. Since chemical concentrations in water samples are independent of the size of the aquatic environment, the final design was scalable for all aquatic systems, from small personal aquariums to large-scale fish farms. Figure 1 shows the operational concept that utilizes standard freshwater test kit chemical solutions for testing the chemicals.

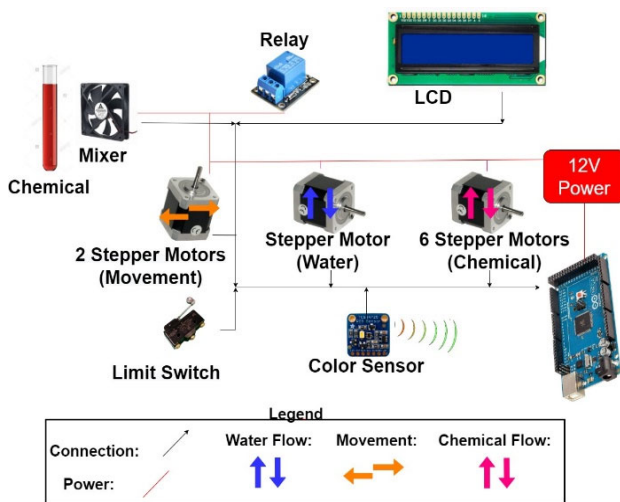


Figure 1. Conceptual block diagram.

The system initiated the measurement process by rinsing the test tube and performing a calibration using clean distilled water. From the display menu, the user could select the testing of the three chemicals individually or all consecutively. Once a test was selected, the chemical dosers precisely dispensed 5 ml of the sample water and the prescribed chemical solutions into a test vial. The stepper motors used here were calibrated to the accurate weight measure of the chemical to be dispensed, which was much more accurate than the drop-counting method required by the standard test kit. The magnetic stirrer underneath the test vial agitated the test tube mixture, allowing a uniform solution within the sample. After the chemical reaction reached equilibrium, the color sensor measured the solution's RGB values, calculated the chemical concentration

based on calibration curves, and displayed the water concentration of the selected chemical. Once the test results were recorded, the test tube contents were disposed of in the waste bin and the vial was automatically rinsed and air dried in preparation for the next use.

Figure 2 shows a representation of the circuit components used in the control of the aquatic monitoring system, illustrating the mechanical, intelligence, and user interface subsections of the printed circuit board that was created for the project.

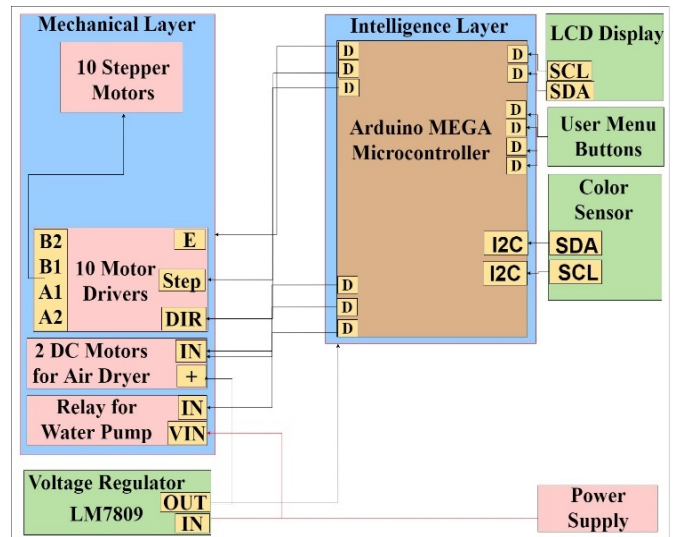


Figure 2. Functional block diagram.

The functional requirements of the monitoring system were separated into five main technical subsections: power, hardware, software, communications, and autonomous performance. Functional requirements were determined by the group using "best use scenarios" that allow for the determination of performance expectations based on a user's experience. The entire system was powered by a 12VDC power supply that was stepped down to 9V and 5V using appropriate voltage regulators. The 12V output was used to power the stepper motors, while the 9V output was used for the stepper motor control signals. The 5V output powered the DC motors, the microcontroller, and the color sensor. Although the system used numerous motors, no more than two motors were operated simultaneously. This operating concept reduced the overall current draw for the system.

The backbone of the aquatic monitoring system was an Arduino MEGA microcontroller coupled with an Adafruit TCS34725 color sensor. The purpose of using a microcontroller was to have a compact integrated circuit designed to govern all the necessary operations needed to run the autonomous system. The Arduino MEGA was the ideal microcontroller, due to the various analog, timing, and communications peripherals that can be used to operate the entire

system. Equally important was the TCS34725 color sensor used to detect the color in the test tube in red, green, and blue, operating as light to digital converters to provide a digital return of red, green, and blue (RGB) color levels. To display the chemical concentrations, an LCD display was mounted on top of the system. The conceptual block diagram in Figure 1 shows the flow of the power, chemicals, and water of the prototype that was built. The purpose of creating the functional block diagram was to ensure an accurate schematic for the hardware engineer to use in creating the overall aquatic monitoring System.

## Functional Design

The functional block diagram in Figure 2 shows each layer, including the components associated with the mechanical, intelligence, and power layers. The aquatic monitoring system required a minimum of three different subsystems: the intelligence subsystem consisting of the Arduino MEGA, the mechanical subsystem consisting of the motors and pumps necessary to produce a flowing prototype, and the power subsystem consisting of the necessary voltage monitoring and regulation. Figure 3 shows a detailed functional block diagram for the configuration of how the color sensor was connected to the Arduino MEGA and how it was powered through the LM7805 voltage regulator.

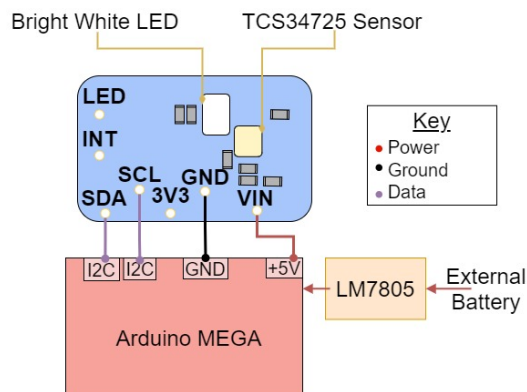


Figure 3. Sensor detailed functional block diagram.

Also in Figure 3, one can see the basic functional breakdown of the Adafruit TCS34725 color sensor. The sensor consisted of two primary components: the white LED and the sensor chip, as well as seven unique I/O ports. When the board is powered, the white LED emits a very bright light that allows the TCS34725 sensor to read color (regardless of ambient light). The four I/O pins utilized were the VIN (5V), ground, SDA (Serial Data), and SCL (Serial Clock) Pins. The Arduino MEGA provided the 5VDC signal required to power the sensor board and its associated ground as well as an I2C I/O data port that was useful for serial communication while processing and displaying the color readings from the sensor.

Figure 4 depicts the detailed functional block diagram that controlled the stepper motors. It consisted of multiple components, such as the Arduino MEGA microcontroller, DRV8825 motor driver, two voltage regulators, an external power supply of 12V, and the stepper motor itself. The stepper motors moved in discrete single steps determined by the program, allowing precise control of the motor position and speed.

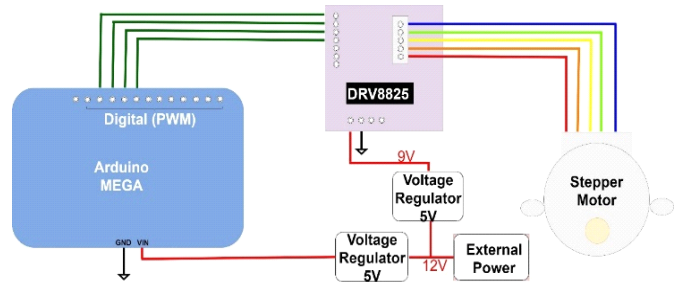


Figure 4. Stepper motors detailed functional block diagram.

Figure 5 shows a detailed functional block diagram of the DC motor, the main component for which was the Arduino MEGA microcontroller, which was used as the control mechanism to move the DC motors via a MOSFET transistor. External power was used to actuate the DC motor. The DC motors were used to provide movement of the sample throughout the process. Figure 6 is a schematic diagram showing an overview of the dosing pumps' components integrated into the aquatic monitoring system.

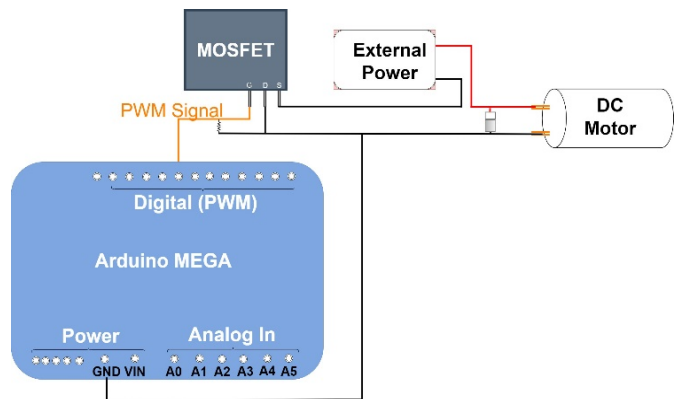


Figure 5. DC motors detailed functional block diagram.

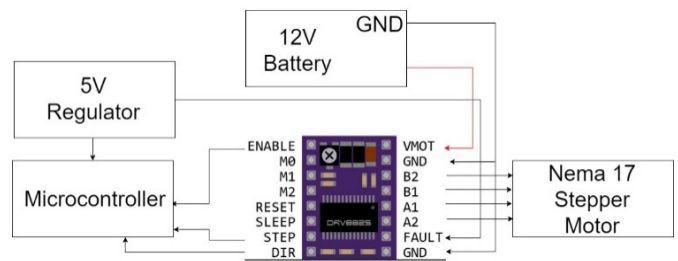


Figure 6. Dosers detailed functional block diagram.

The chemical doser was a peristaltic pump driven by a NEMA 17 stepper motor that was controlled by a DRV8825 driver board. The driver board increased the precision from full step to 132 steps, meaning that the resolution of step size was maximized 32 times and was configured using the M0-M2 pins. The stepper motor was powered by 12V through the driver board, while 5V powered the microcontroller and the driver board. The driver's inputs (power, enable, step, and direction pin) and the outputs (A1, A2, B1, and B2 stepper pins) were connected to the microcontroller and stepper motor, respectively.

## Performance Specifications

The printed circuit board (PCB) design was generated using Altium, an industry standard tool for PCB layout. Design rules based on size, power consumption, and manufacturability were used in the design of the PCB. The goal was to minimize the layer count, via count, as well as board size. Figure 7 shows the final top layer of the PCB.

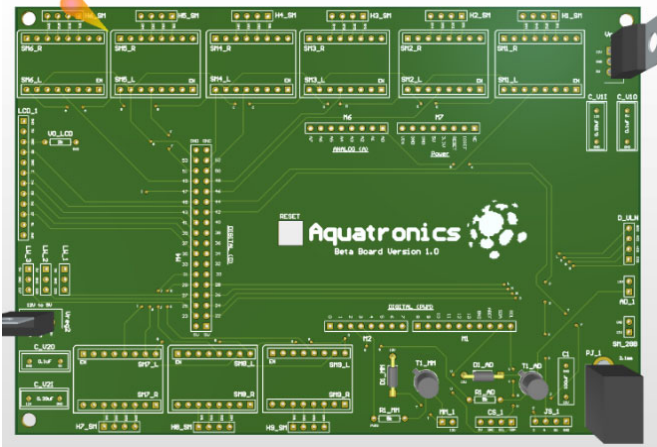


Figure 7. Top layer of the PCB.

The Aquatic Monitoring System was designed to withstand minimal water splashing and be classified as a water-resistant device. Although the final cover was not produced, Solid Works models were created that would meet the water incursion expectation. The software was expected to run without error and control the performance of the necessary functions (e.g., moving motors, reading color sensor, and processing received data) without impeding each chemical test flow. The most critical feature of the entire system was the calibration of the chemical concentration in the sample to an expected accuracy of parts per million (ppm).

## Test Matrix

A test matrix was created to ensure that all hardware and software were integrated properly. Due to the size of the matrix, each of the sections was broken down into timing, automation, features, installation, and power (see Tables

1-4). Logical steps were used in determining if the test passed or failed. Only one test was chosen for inclusion here as demonstration of the testing process. All tests listed in Tables 1-4 were completed successfully. Test 2 (see Table 1) verified that the system performed all chemical tests sequentially. The following steps were performed to test full functionality.

1. Check to ensure motors are in starting position.
2. Go through user interface features and click through each of the options.
3. Select all three chemicals to be tested by scrolling left or right throughout the main menu and choosing "Select Chemicals" and then selecting all.
4. Verify that the LCD screen is easy to navigate, follows a standard layout, and is easy to use for the target market.
5. Run the test by clicking the joystick and selecting "Run."
6. Verify the system responds in a timely manner.
7. Validate that the chemical value displayed matched the calibration fluid to  $\pm 1$  ppm.
8. Verify that all chemical waste has been disposed of properly and that all moving parts were returned to the original location.
9. Check that the option to clean is listed.
10. Repeat this 50 times to ensure that the system can measure and read without error and is repeatable.

## Results & Future Work

The results from the autonomous system showed that it is possible to accurately dose a series of vials to read ammonia, nitrate, and nitrite RGB values. Designing a system on this engineering technology level required significant capability in mechanical, electrical, and software development as applied to motors and microcontrollers. One of the problems present in the final prototype was an unexplained variability in the baseline of the color readings that caused an extensive daily calibration to ensure correct chemical readings. The RGB values of the color sensor baseline (using clean water) were sometimes high, low, or mid-range, making it harder to pinpoint the exact concentration the autonomous system was reading. After significant analysis using Python and Excel spreadsheets, the team identified the relationship between the color data to read a concentration with a  $\pm 0.75$  ppm error, well within the error margin expected from the prototype. Table 5 shows the Excel analysis of three consecutive tests of clear water and the associated RGB values versus Lux readings, which demonstrates the baseline shifts encountered.

After calibration, the result of the automated chemical monitor showed a good correlation to chemical test strip measurements (visually verified) as well as sufficient repeatability of results (again, compared to repeatability of visual inspection of chemical test strips). Figures 8 and 9 show the front and top views of the final prototype, respectively.



Table 1. Test matrix—Timing.

Test Matrix	Timing						
	No moving parts	Response time after selection	Time it takes to dose and mix	Color sensor reads within a certain time	Moors hold enough for color sensor to read	Total time for test to finish	Total time for system to flush out and be cleaned
Test 1: Visible Inspection	X						
Test 2: Performance Test to verify feature is included		X	X	X	X	X	X
Test 3: Functional test to verify PWM	X	X	X	X	X	X	X
Test 4: Measurement & Readings				X			
Test 5: Performance test to verify Power							
Test 6: Performance test to verify continuity to $\mu$ C	X	X	X	X	X	X	X
Test 7: Functional test to verify dosing accuracy			X				
Test 8: Functional test to verify dosing repeatability			X				
Test 9: Functional test to verify flush system							X
Test 10: Functional test to verify magnetic mixer			X	X			
Test 11: Functional test to verify limit switches	X	X	X		X	X	X
Test 12: Functional test to verify color sensor accuracy			X				
Test 13: Performance test to verify color sensor repeatability			X				

Table 2. Test matrix—Automation.

Test Matrix	Automation					
	Motors move to selected chemicals	Chemicals are dosed based on chemical selected	Magnetic mixer mixes each vial	Color sensor reads correct vial(s)	Flush system cleans vial(s)	Motor returns to original position
Test 1: Visible Inspection						X
Test 2: Performance Test to verify feature is included	X	X	X	X	X	X
Test 3: Functional test to verify PWM	X	X		X	X	X
Test 4: Measurement & Readings	X	X		X		
Test 5: Performance test to verify Power	X	X	X	X	X	X
Test 6: Performance test to verify continuity to $\mu$ C	X	X	X	X	X	X
Test 7: Functional test to verify dosing accuracy		X				
Test 8: Functional test to verify dosing repeatability		X				
Test 9: Functional test to verify flush system					X	
Test 10: Functional test to verify magnetic mixer	X		X	X		
Test 11: Functional test to verify limit switches	X	X	X		X	X
Test 12: Functional test to verify color sensor accuracy			X			
Test 13: Performance test to verify color sensor repeatability			X			

Table 3. Test matrix—Features.

Test Matrix	Features										
	Ammonia	Nitrate	Nitrite	Clean	Display estimated finish time	Display RGB values	Display if any chemicals are toxic	Display that vials are cleaned	Verify ease of navigation	Verify sample screens	System shall be easy to use
Test 1: Visible Inspection	X	X	X	X	X	X	X	X	X	X	X
Test 2: Performance Test to verify feature is included	X	X	X	X					X	X	X
Test 3: Functional test to verify PWM											
Test 4: Measurement & Readings	X	X	X	X	X	X					
Test 5: Performance test to verify Power											
Test 6: Performance test to verify continuity to $\mu$ C	X	X	X	X	X	X	X	X	X	X	X
Test 7: Functional test to verify dosing accuracy	X	X	X								
Test 8: Functional test to verify dosing repeatability	X	X	X								
Test 9: Functional test to verify flush system				X				X			
Test 10: Functional test to verify magnetic mixer	X	X	X		X	X					
Test 11: Functional test to verify limit switches											
Test 12: Functional test to verify color sensor accuracy	X	X	X		X	X					
Test 13: Performance test to verify color sensor repeatability	X	X	X		X	X					

Table 4. Test matrix—Installation & Power.

Test Matrix	Installation			Power			
	Location of system on a small fish tank	Dosing tube connected to the fish tank via 3D printed piece	User interface setup instructions	Powered by an AC/DC Adapter switching power supply	Ability to regulate US standard wall power	Verify power to all components	enough power supplied to all components
Test 1: Visible Inspection	X	X	X				
Test 2: Performance Test to verify feature is included	X	X	X	X	X	X	X
Test 3: Functional test to verify PWM							
Test 4: Measurement & Readings					X	X	X
Test 5: Performance test to verify Power					X	X	X
Test 6: Performance test to verify continuity to $\mu$ C					X	X	X
Test 7: Functional test to verify dosing accuracy							
Test 8: Functional test to verify dosing repeatability							
Test 9: Functional test to verify flush system						X	
Test 10: Functional test to verify magnetic mixer						X	
Test 11: Functional test to verify limit switches				X	X	X	X
Test 12: Functional test to verify color sensor accuracy						X	
Test 13: Performance test to verify color sensor repeatability						X	

Table 5. Test data.

	RGB Data (Day 1)					RGB Data (Day 2)					RGB Data (Day 3)			
	Red	Green	Blue	LUX		Red	Green	Blue	LUX		Red	Green	Blue	LUX
0ppm	1610	1800	1522	1202		1364	1404	1011	1039		1312	1387	1002	1029
0ppm	1612	1793	1522	1193		1314	1366	994	1001		1349	1410	1010	1049
0ppm	1610	1791	1529	1185		1333	1395	1021	1021		1366	1449	1045	1078

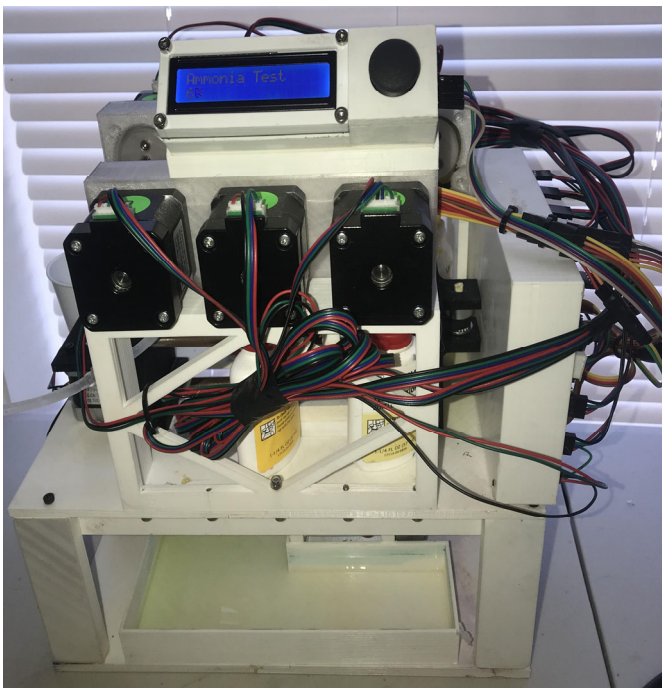


Figure 8. Final prototype front view.

To further develop the system into a commercial product, additional debugging efforts will be needed to address the stability issues in the color sensor that were temporarily fixed using software algorithms. For this project's future work, the authors plan to set up the autonomous system at a professional aquaculture facility, where it will monitor the ammonia, nitrate, and nitrite of a large freshwater prawn tank. The system is expected to report tank concentrations of each of the toxic by-products of the nitrogen cycle to better manage the tank without having to deal with paper test strips and physically observing the color samples. The chemical monitoring system described here could be implemented on any aquatic system, as the team tried to make the product as scalable as possible for both small and large fish tanks for use in the future.

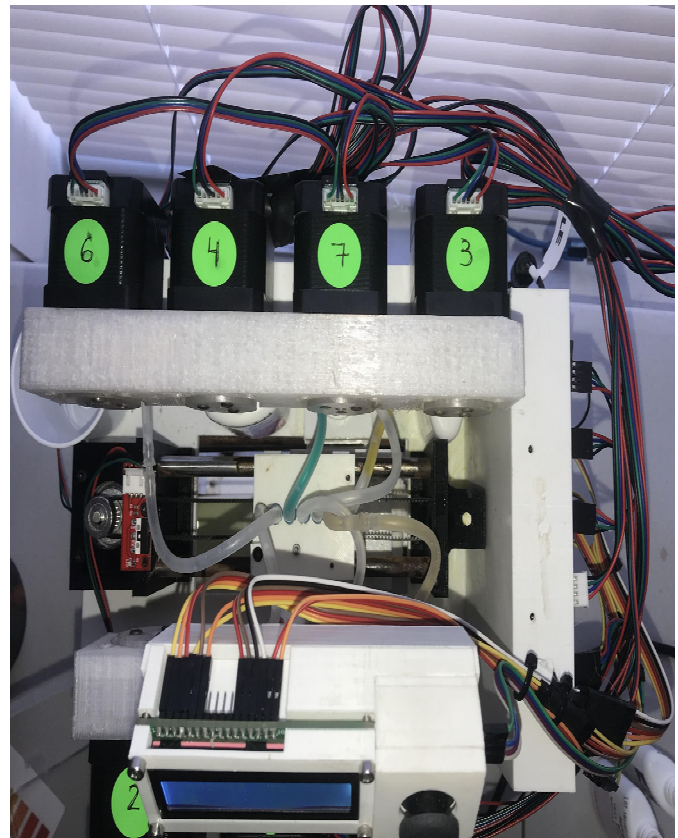


Figure 9. Final prototype top view.

## Conclusions

Creating a waterproof automated system that measures ammonia, nitrite, and nitrate levels of an aquatic environment could revolutionize the chemical sensing process used throughout the aquaculture industry and save significant time and effort. The capstone team successfully finished the working prototype and acquired significant useful data to facilitate future development.

---

## References

- Boyd, C. E. (2019). *Nitrogen a limiting factor in aquaculture production*. Global Seafood Alliance. <https://www.aquaculturealliance.org/advocate/nitrogen-a-limiting-factor-in-aquaculture-production>
- Elsokah, M., & Sakah, M. (2019, March 24-26). *Next Generation of Smart Aquaponics with Internet of Things Solution* [Conference presentation]. IEEE. 19<sup>th</sup> International Conference on Sciences and Techniques of Automatic Control and Computer Engineering (STA), Sousse, Tunisia. 106-111. 10.1109/STA.2019.8717280.
- Ertör, I. (2018). *Fish farming at industrial scale: a Turkish case study*. <https://theconversation.com/fish-farming-at-industrial-scale-a-turkish-case-study-105142>
- Goddek, S., Joyce, A., Kotzen, B., & Burnell, G. (2019). *Aquaponic Food Production Systems, Combined Aquaculture and Hydroponic Production Technologies for the Future*. Springer Open.
- Lehane, S. (2013). *Fish for the Future: Aquaculture and Food Security*. <https://apo.org.au/node/35413>
- Marine Fisheries & Aquaculture Series: Farming The Seas – Shrimp Aquaculture: Case Study. (2002-2003). PBS. <https://www.pbs.org/emptyoceans/educators/index.html>

## Biographies

**JADE CHAPMAN** is a student in Electronic Systems Engineering Technology department at Texas A&M University. Her experience in the engineering field ranges from undergraduate research with faculty working with active and passive RFID and Bluetooth Low Energy, working as a teaching assistant and lead coder in the semiconductor testing lab, several summer internships including with Avinext and Reynolds & Reynolds, and much more. Jade plans to graduate in December, 2020, and continue her education in pursuit of a Master's degree in Electronic Systems Engineering Technology, while carrying out a professional internship with Avinext until graduation in May 2022. Jade may be reached at [jchapman12@tamu.edu](mailto:jchapman12@tamu.edu)

**KEVIN ZHANG** is a fourth-year student in the Bachelor of Science Electronic Systems Engineering Technology program at Texas A&M University. Kevin will begin working full-time in 2021 doing telecom for Oncor Electric Delivery. Kevin may be reached at [zhang-719795740@tamu.edu](mailto:zhang-719795740@tamu.edu)

**GAGE ARTER** is a fourth-year student in the Bachelor of Science Electronic Systems Engineering Technology program at Texas A&M University. His experience in the engineering field ranges from undergraduate research under Dr. Zoghi working with active and passive RFID and Bluetooth Low Energy and working as a lab instructor for TAMU General Engineering Department. Gage will begin working full-time in 2021 doing telecom for Oncor Electric Delivery. Gage may be reached at [gagearter@tamu.edu](mailto:gagearter@tamu.edu)

**TRUC LE** is a fourth-year student in the Bachelor of Science Electronic Systems Engineering Technology program at Texas A&M University with a minor in Cyber-Security. His related coursework includes digital electronics, circuit analysis, microcontroller architecture, and advanced local and metropolitan area networks, as he hopes to connect his love for electronics into a career choice. He is originally from Da Nang, Vietnam, and he moved to Houston, Texas, to be the first one in his family to graduate from college. He has earned a Yellow Belt in Lean Six Sigma by elevating the level of operations in improving performance by systematically reducing variation. In his free time, Truc likes to build and design simple electronic devices for entertainment used to protect children/disabled individuals from accessing high voltage outlets. Truc may be reached at [tle91@tamu.edu](mailto:tle91@tamu.edu)

**RAINER FINK** received BS, MS, and PhD degrees in biomedical engineering from Texas A&M University (TAMU). After receiving his PhD degree, he simultaneously taught analog electronics in the Bioengineering Program and the Department of Engineering Technology at TAMU. In 1996, he joined the Electronics Engineering Technology Faculty at TAMU as an assistant professor, and he is now an associate professor. He is the Director of the Texas Instruments Mixed-Signal Test Laboratory at TAMU. He is also a Research Adjunct Professor of Electrical Engineering at the University of Arkansas, Fayetteville. His research activities include mixed-signal testing, analog circuit design, and biomedical electronics. Dr. Fink was the 1999-2000 Monague Center for Teaching Excellence Scholar. Rainer may be reached at [fink@tamu.edu](mailto:fink@tamu.edu)

**BEN ZOGHI** is the Victor H. Thompson chair professor of Electronics System Engineering Technology at Texas A&M. He directs the RFID/Sensor Lab and the new online professional Master of Engineering in Technical Management program. A member of the Texas A&M University faculty for 33 years, he has distinguished himself as a teacher, writer, and researcher, and has been honored for his teaching excellence by the College and the Texas A&M University Association of Former Students. Ben's academic and professional degrees are from Texas A&M (PhD), The Ohio State University (MSEE), and Seattle University (BSEE). Dr. Zoghi may be reached at [zoghi@tamu.edu](mailto:zoghi@tamu.edu)

# INSTRUCTIONS FOR AUTHORS: MANUSCRIPT FORMATTING REQUIREMENTS

The INTERNATIONAL JOURNAL OF ENGINEERING RESEARCH AND INNOVATION is an online/print publication designed for Engineering, Engineering Technology, and Industrial Technology professionals. All submissions to this journal, submission of manuscripts, peer-reviews of submitted documents, requested editing changes, notification of acceptance or rejection, and final publication of accepted manuscripts will be handled electronically. The only exception is the submission of separate high-quality image files that are too large to send electronically.

All manuscript submissions must be prepared in Microsoft Word (.doc or .docx) and contain all figures, images and/or pictures embedded where you want them and appropriately captioned. Also included here is a summary of the formatting instructions. You should, however, review the sample Word document on our website (<http://ijeri.org/formatting-guidelines>) for details on how to correctly format your manuscript. The editorial staff reserves the right to edit and reformat any submitted document in order to meet publication standards of the journal.

The references included in the References section of your manuscript must follow APA-formatting guidelines. In order to help you, the sample Word document also includes numerous examples of how to format a variety of scenarios. Keep in mind that an incorrectly formatted manuscript will be returned to you, a delay that may cause it (if accepted) to be moved to a subsequent issue of the journal.

1. **Word Document Page Setup:** Two columns with ¼" spacing between columns; top of page = ¾"; bottom of page = 1" (from the top of the footer to bottom of page); left margin = ¾"; right margin = ¾".
2. **Paper Title:** Centered at the top of the first page with a 22-point Times New Roman (Bold), small-caps font.
3. **Page Breaks:** Do not use page breaks.
4. **Figures, Tables, and Equations:** All figures, tables, and equations must be placed immediately after the first paragraph in which they are introduced. And, each must be introduced. For example: "Figure 1 shows the operation of supercapacitors." "The speed of light can be determined using Equation 4:"
5. **More on Tables and Figures:** Center table captions

above each table; center figure captions below each figure. Use 9-point Times New Roman (TNR) font. Italicize the words for table and figure, as well as their respective numbers; the remaining information in the caption is not italicized and followed by a period—e.g., "*Table 1*. Number of research universities in the state." or "*Figure 5*. Cross-sectional aerial map of the forested area."

6. **Figures with Multiple Images:** If any given figure includes multiple images, do NOT group them; they must be placed individually and have individual minor captions using, "(a)" "(b)" etc. Again, use 9-point TNR.
7. **Equations:** Each equation must be numbered, placed in numerical order within the document, and introduced—as noted in item #4.
8. **Tables, Graphs, and Flowcharts:** All tables, graphs, and flowcharts must be created directly in Word; tables must be enclosed on all sides. The use of color and/or highlighting is acceptable and encouraged, if it provides clarity for the reader.
9. **Textboxes:** Do not use text boxes anywhere in the document. For example, table/figure captions must be regular text and not attached in any way to their tables or images.
10. **Body Fonts:** Use 10-point TNR for body text throughout (1/8" paragraph indentation); indent all new paragraphs as per the images shown below; do not use tabs anywhere in the document; 9-point TNR for author names/affiliations under the paper title; 16-point TNR for major section titles; 14-point TNR for minor section titles.



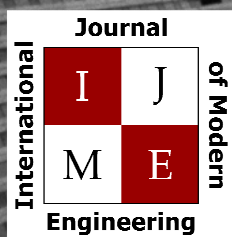
11. **Personal Pronouns:** Do not use personal pronouns (e.g., "we" "our" etc.).
12. **Section Numbering:** Do not use section numbering of any kind.
13. **Headers and Footers:** Do not use either.

14. **References in the Abstract:** Do NOT include any references in the Abstract.
15. **In-Text Referencing:** For the first occurrence of a given reference, list all authors—last names only—up to seven (7); if more than seven, use “et al.” after the seventh author. For a second citation of the same reference—assuming that it has three or more authors—add “et al.” after the third author. Again, see the *sample Word document* and the *formatting guide for references* for specifics.
16. **More on In-Text References:** If you include a reference on any table, figure, or equation that was not created or originally published by one or more authors on your manuscript, you may not republish it without the expressed, written consent of the publishing author(s). The same holds true for name-brand products.
17. **End-of-Document References Section:** List all references in alphabetical order using the last name of the first author—last name first, followed by a comma and the author’s initials. Do not use retrieval dates for websites.
18. **Author Biographies:** Include biographies and current email addresses for each author at the end of the document.
19. **Page Limit:** Manuscripts should not be more than 15 pages (single-spaced, 2-column format, 10-point TNR font).
20. **Page Numbering:** Do not use page numbers.
21. **Publication Charges:** Manuscripts accepted for publication are subject to mandatory publication charges.
22. **Copyright Agreement:** A copyright transfer agreement form must be signed by all authors on a given manuscript and submitted by the corresponding author before that manuscript will be published. Two versions of the form will be sent with your manuscript’s acceptance email.
23. **Submissions:** All manuscripts and required files and forms must be submitted electronically to Dr. Philip D. Weinsier, manuscript editor, at [philipw@bgsu.edu](mailto:philipw@bgsu.edu).
24. **Published Deadlines:** Manuscripts may be submitted at any time during the year, irrespective of published deadlines, and the editor will automatically have your manuscript reviewed for the next-available issue of the journal. Published deadlines are intended as “target” dates for submitting new manuscripts as well as revised documents. Assuming that all other submission conditions have been met, and that there is space available in the associated issue, your manuscript will be published in that issue if the submission process—including payment of publication fees—has been completed by the posted deadline for that issue.

Missing a deadline generally only means that your manuscript may be held for a subsequent issue of the journal. However, conditions exist under which a given manuscript may be rejected. Always check with the editor to be sure. Also, if you do not complete the submission process (including all required revisions) within 12 months of the original submission of your manuscript, your manuscript may be rejected or it may have to begin the entire review process anew.

Only one form is required. Do not submit both forms!

The form named “paper” must be hand-signed by each author. The other form, “electronic,” does not require hand signatures and may be filled out by the corresponding author, as long as he/she receives written permission from all authors to have him/her sign on their behalf.



[www.ijme.us](http://www.ijme.us)

Print ISSN: 2157-8052  
Online ISSN: 1930-6628



[www.iajc.org](http://www.iajc.org)

## INTERNATIONAL JOURNAL OF MODERN ENGINEERING

### ABOUT IJME:

- IJME was established in 2000 and is the first and official flagship journal of the International Association of Journal and Conferences (IAJC).
- IJME is a high-quality, independent journal steered by a distinguished board of directors and supported by an international review board representing many well-known universities, colleges and corporations in the U.S. and abroad.
- IJME has an impact factor of **3.00**, placing it among the top 100 engineering journals worldwide, and is the #1 visited engineering journal website (according to the National Science Digital Library).

### OTHER IAJC JOURNALS:

- The International Journal of Engineering Research and Innovation (IJERI)  
For more information visit [www.ijeri.org](http://www.ijeri.org)
- The Technology Interface International Journal (TIIJ).  
For more information visit [www.tiij.org](http://www.tiij.org)

### IJME SUBMISSIONS:

- Manuscripts should be sent electronically to the manuscript editor, Dr. Philip Weinsier, at [philipw@bgsu.edu](mailto:philipw@bgsu.edu).

For submission guidelines visit  
[www.ijme.us/submissions](http://www.ijme.us/submissions)

### TO JOIN THE REVIEW BOARD:

- Contact the chair of the International Review Board, Dr. Philip Weinsier, at [philipw@bgsu.edu](mailto:philipw@bgsu.edu).

For more information visit  
[www.ijme.us/ijme\\_editorial.htm](http://www.ijme.us/ijme_editorial.htm)

### INDEXING ORGANIZATIONS:

- IJME is indexed by numerous agencies. For a complete listing, please visit us at [www.ijme.us](http://www.ijme.us).

### Contact us:

**Mark Rajai, Ph.D.**

Editor-in-Chief  
California State University-Northridge  
College of Engineering and Computer Science  
Room: JD 4510  
Northridge, CA 91330  
Office: (818) 677-5003  
Email: [mrajai@csun.edu](mailto:mrajai@csun.edu)



[www.tiij.org](http://www.tiij.org)



[www.ijeri.org](http://www.ijeri.org)

The International Journal of Engineering Research & Innovation (IJERI) is the second official journal of the International Association of Journals and Conferences (IAJC). IJERI is a highly-selective, peer-reviewed print journal which publishes top-level work from all areas of engineering research, innovation and entrepreneurship.

## **IJERI Contact Information**

General questions or inquiry about sponsorship of the journal should be directed to:

Mark Rajai, Ph.D.

Founding and Editor-In-Chief

Office: (818) 677-5003

Email: [editor@ijeri.org](mailto:editor@ijeri.org)

Department of Manufacturing Systems Engineering & Management

California State University-Northridge

18111 Nordhoff St.

Room: JD3317

Northridge, CA 91330